NACA TN 2466

NATIONAL ADVISORY COMMITTEE FOR AERONAUTICS

TECHNICAL NOTE 2466

A GENERAL CORRELATION OF TEMPERATURE PROFILES DOWNSTREAM OF A HEATED-AIR JET DIRECTED PERPENDICULARLY TO AN AIR STREAM

By Edmund E. Callaghan and Robert S. Ruggeri

Lewis Flight Propulsion Laboratory
Cleveland, Ohio

PROPERTY FAIRCHILD
ENGINEERING LIBRARY

Washington
September 1951

NATIONAL ADVISORY COMMITTEE FOR AERONAUTICS

TECHNICAL NOTE 2466

A GENERAL CORRELATION OF TEMPERATURE PROFILES DOWNSTREAM OF A HEATED-AIR JET DIRECTED PERPENDICULARLY TO AN AIR STREAM

2221

By Edmund E. Callaghan and Robert S. Ruggeri

SUMMARY

An experimental investigation was conducted to determine the temperature profile downstream of a heated-air jet directed perpendicularly to an air stream. The profiles were determined at several positions downstream of the jet as functions of jet density, jet velocity, free-stream density, free-stream velocity, jet temperature, and orifice flow coefficient.

A method is presented which yields a good approximation of the temperature profile in terms of dimensionless parameters of the flow and geometric conditions.

INTRODUCTION

The heating of an air stream by means of an air jet directed perpendicularly to the air stream is reported in references 1 and 2. These investigations were conducted to determine the penetration of a jet into the air stream at various downstream positions as a function of the jet and stream-flow conditions and of the size and shape of the orifices from which the jet issued. The practical application of such a heating system requires a knowledge of the temperature profile at any point downstream of the orifice as well as the penetration of the jet into the air stream.

An investigation was therefore conducted in a 2- by 20-inch tunnel at the NACA Lewis laboratory to determine the temperature profile in the plane of a jet at several positions downstream of a jet directed perpendicularly to an air stream. Four heated air jets were investigated for a range of free-stream velocities, jet total temperatures, and jet total pressures.

APPARATUS AND PROCEDURE

The orifices used in the investigation were circular thin-plate orifices with diameters of 0.250, 0.385, 0.500, and 0.625 inch. Each orifice was investigated over a range of pressure ratios (ratio of jet total pressure to outlet static pressure) from 1.20 to 3.70 for jet total temperatures of approximately 200°, 300°, and 400° F at free-stream velocities of 160, 275, and 390 feet per second. Air for the jets was obtained by passing high-pressure air through an electric heater and into a plenum chamber, the upper wall of which contained the orifices as shown in figure 1.

2221

The temperature profiles were measured at three positions downstream of the orifice center line by means of thermocouple rakes. A rake consisting of 22 thermocouple probes spaced 0.500 inch apart was permanently mounted at the rearmost position (20.31 in.) downstream of the orifice center line. A moveable rake consisting of 33 thermocouple probes spaced 0.250 inch apart was used to measure the temperature profiles at stations 4.81 and 11.81 inches downstream of the orifice center line.

The tunnel boundary layer was removed by suction upstream of the orifice to minimize tunnel-wall boundary-layer effects. (See fig. 1.)

SYMBOLS

The following symbols are used in this report:

a,b	exponents for correlating X_1
d,e,f	exponents for correlating X_2
C	flow coefficient, dimensionless
D_j	diameter of orifice, inches
l	depth of jet penetration into air stream as defined in reference 1, inches
M_L	slope of lower portion of temperature profile curve, inches per °F
M_U	slope of upper portion of temperature profile curve, inches per °F
s	distance downstream of orifice center line or mixing distance, inches

T_j	total temperature of jet, $^{\circ}R$
T_0	total temperature of free stream, $^{\circ}R$
ΔT	total-temperature rise above free-stream total temperature measured at any point X for given temperature profile, $^{\circ}F$
ΔT_m	maximum total-temperature rise above free-stream total temperature, $^{\circ}F$
V_j	velocity of jet at vena contracta, feet per second
V_0	velocity of free stream, feet per second
w	width of jet boundary at any point downstream of orifice center line, inches
X	distance normal to surface of model, inches
X_1	depth of jet penetration into air stream as determined by intersection of line of slope M_U with value of $\Delta T = 0$, inches
X_2	value of X as determined by the intersection of line of slope M_L with value of $\Delta T = \Delta T_m$, inches
θ_L	arc tan of M_L
θ_U	arc tan of M_U
μ_j	viscosity of jet at vena contracta, slugs per foot-second
μ_0	viscosity of free stream, slugs per foot-second
ρ_j	mass density of jet at vena contracta, slugs per cubic foot
ρ_0	mass density of free stream, slugs per cubic foot
$\varphi_1 \ldots \varphi_4$	correlation parameters

METHOD OF ANALYSIS

The dimensional analysis and experimental results of reference 1 indicate that the penetration coefficient l/D_j can be correlated in terms of the jet Reynolds number $\rho_j V_j D_j/\mu_j$, the viscosity ratio μ_j/μ_0, the density ratio ρ_j/ρ_0, the velocity ratio V_j/V_0, the

mixing distance to diameter ratio s/D_j, and a width coefficient w/D_j. Although the parameters are in most cases self explanatory, the width coefficient can have two significantly different meanings. If the jet is confined by the tunnel walls (as in reference 1 and in this report), the width coefficient is a function of the tunnel dimensions. If the jet is unconfined, the width coefficient depends on the actual jet width at the point of interest and is independent of the tunnel dimensions. A discussion of the proper use of the width coefficient is presented in the section "Extrapolation of Results to Wider Range of Variables."

2221

The results of reference 2 show that the small effect of jet Reynolds number is eliminated if the actual orifice diameter D_j is replaced by the effective orifice diameter $\sqrt{C}D_j$. In the analysis data, it is sometimes more desirable to use the ratio $s/\sqrt{C}D_j$ rather than s/D_j. In order to differentiate between them, s/D_j is defined as the mixing distance to diameter ratio and $s/\sqrt{C}D_j$ as the ratio of the mixing distance to effective diameter.

The purpose of the analysis presented herein was to obtain a method by which the temperature profile downstream of a heated-air jet directed perpendicularly to an air stream may be predicted if the flow parameters and geometry are known.

In an over-all study of the profile data, certain consistent characteristics of the profiles that suggested a simplified means for correlating the data were observed. These characteristics were noted in the study of the profiles at jet-pressure ratios greater than choking for a particular orifice diameter, rake position, free-stream velocity, and jet total temperature. A set of typical profiles is shown in figure 2(a). It is evident from the figure that the profiles are quite similar, the upper and lower portions consisting of approximately linear segments that remain parallel for the values of jet-pressure ratio shown. For a particular value of orifice diameter, rake position, free-stream velocity, and jet total temperature, the maximum temperature rise decreased slightly with decreasing jet-pressure ratio. A study of the profiles for other diameters, rake stations, and free-stream velocities showed the same characteristics for jet-pressure ratios greater than 1.87. It was therefore decided to approximate the profiles with three straight lines as shown in figure 2(b); and because the upper and lower slopes of the temperature profiles are independent of pressure ratio for values greater than choking, the analysis was limited to jet-pressure ratios greater than 1.87.

The height of intersection of the upper slope (fig. 2(b)) with the free-stream temperature is defined as the depth of penetration X_1. This definition differs from that in reference 1 wherein the depth of

penetration l was defined as the point at which the temperature profile returns to 1° above the free-stream total temperature. As a consequence, the penetration as defined in reference 1 is slightly greater than that presented in this report. The height of intersection of the lower slope with the maximum temperature rise is defined as X_2, the maximum temperature rise ΔT_m and the slopes of the upper and lower portion of the profile curve M_U and M_L, respectively.

2221

The depth of penetration may be correlated in terms of the dimensionless penetration coefficient and the parameters previously stated. The slopes and the maximum temperature rise may be correlated by similar means provided that they are expressed in dimensionless form. This correlation requires the introduction of a temperature into the dimensional analysis as another variable. Because both the slope and the temperature rise are based on temperature differences, a temperature difference would apparently best fulfill this requirement. The only temperatures involved in the investigation are the stream temperature and the jet temperature; therefore the temperature difference T_j-T_0 was included as the additional variable. The use of this temperature difference results in slope coefficients $M_L(T_j-T_0)/D_j$ and $M_U(T_j-T_0)/D_j$ and a temperature rise coefficient $\Delta T_m/(T_j-T_0)$, which are functions of the same dimensionless parameters as the penetration coefficient.

The procedure for correlation used in this investigation is similar to that previously described in references 1 and 2. The parameters and the flow coefficients were calculated by the method presented in reference 3. The correlation of data by means of parameters obtained from a dimensional analysis usually requires that all but one of the parameters be held constant, and by this means the effect of its variation on a coefficient may be studied.

RESULTS AND DISCUSSION

Correlation of Penetration Coefficient $X_1/\sqrt{C}D_j$ with Dimensionless Parameters

The variation of the penetration coefficient $X_1/\sqrt{C}D_j$ with density ratio was investigated for a single orifice diameter, rake position, free-stream velocity, and jet total temperature. Because the jet pressure ratio was always greater than the choking value and the jet total temperature was held constant, the jet velocity remained constant. All parameters, both flow and geometric, were therefore invariable with the exception of the density ratio.

The variation of penetration coefficient with density ratio for the 0.385-inch-diameter orifice at the 4.81-inch rake position is shown in figure 3 for a jet total temperature of 860° R and three velocity ratios. The relation of the penetration coefficient to the density ratio may be determined and algebraically expressed by a method similar to that used in reference 1 as follows:

$$\frac{X_1}{\sqrt{CD_j}} = \varphi_1 \left(\frac{\rho_j}{\rho_0}\right)^{0.57} \tag{1}$$

2221

where φ_1 is a known constant dependent on the velocity ratio. The variation of φ_1 with velocity ratio is then plotted as shown in figure 4, and again the algebraic relation is determined. For these data φ_1 can be expressed as

$$\varphi_1 = \varphi_2 \left(\frac{V_j}{V_0}\right)^{0.64} \tag{2}$$

The penetration coefficient can therefore be linearly correlated at the particular value of rake station, diameter, and jet total temperature used by means of the expression $(\rho_j/\rho_0)^{0.57} (V_j/V_0)^{0.64}$. The same procedure is then employed for correlation of the penetration coefficient with density ratio and velocity ratio with the same orifice diameter at the other rake positions.

As a result of these correlations, it was found that the penetration coefficient could be correlated by an expression having the same exponents for all three rake positions (constant values of s/D_j) as shown in figure 5. The curve obtained for each rake position shows the effect that the mixing distance to diameter ratio has on the penetration coefficient; its effect is determined by plotting the slopes of the lines as functions of the mixing distance to diameter ratio (fig. 6) and expressing the relation as follows:

$$\varphi_2 = \varphi_3 \, (s/D_j)^{0.26} \tag{3}$$

If φ_2 is then substituted in equation (2), all the data for the 0.385-inch-diameter orifice and a jet total temperature of 860° R can be correlated using the expression

$$(\rho_j/\rho_0)^{0.57} \quad (V_j/V_0)^{0.64} \quad (s/D_j)^{0.26}$$

A further refinement of this parameter, which results in better correlation of the data, was achieved by the substitution of the effective diameter $\sqrt{CD_j}$ for the actual diameter D_j. The final parameter for the 0.385-inch-diameter orifice at a jet total temperature of 860° R (fig. 7) is therefore

$$(\rho_j/\rho_0)^{0.57} \quad (V_j/V_0)^{0.64} \quad (s/\sqrt{CD_j})^{0.26}$$

2221

The data for the other orifice diameters were correlated by the foregoing procedure and similar correlation parameters resulted. The value of the exponents of the density ratio and the velocity ratio, however, decreased with decreasing diameter indicating an effect of width coefficient w/D_j. The variation of these exponents with the width coefficient (fig. 8) indicates that the exponents become asymptotic to a finite value for high width coefficients. The exponent of the ratio of the mixing distance to the effective diameter $s/\sqrt{CD_j}$ was found to be a constant for all diameters.

The correlation of the data obtained at various diameters may be accomplished by plotting the penetration coefficient as a function of the parameter $(\rho_j/\rho_0)^a \quad (V_j/V_0)^b \quad (s/\sqrt{CD_j})^{0.26}$ (fig. 7) and using the particular exponents that apply. The four lines obtained represent the various width coefficients and further correlation is obtained by plotting the slopes of these lines φ_3 as a function of the width coefficient as shown in figure 9 for a jet total temperature of 860° R.

It is evident that the correlation parameter φ_3 increases with increasing width coefficient and that it becomes asymtotic to a finite value of φ_3 at the higher width coefficients. Therefore, φ_3 cannot be readily expressed as a simple power function. The same result can be obtained by use of the curve plotted for $T_j/T_0 = 1.63$ in figure 9. The over-all parameter for final correlation of all orifice diameters at all rake stations investigated and one jet total temperature is

$$\varphi_3 \quad (\rho_j/\rho_0)^a \quad (V_j/V_0)^b \quad (s/\sqrt{CD_j})^{0.26}$$

which results in a linear variation with penetration coefficient as shown in figure 10.

A similar analysis of the other jet temperatures yielded the identical relations for the exponents of density ratio, velocity ratio, and ratio of mixing distance to effective diameter. The term φ_3, however, was slightly affected by jet total temperature (fig. 9) and the three curves of φ_3 given as functions of width coefficient obtained for the three temperatures show that φ_3 decreases slightly with decreasing jet total temperature. This variation of φ_3 with jet total temperature indicates that the previously neglected viscosity-ratio parameter μ_j/μ_0 has a small effect. For the range of temperatures investigated, the viscosity of air is proportional to a power of the absolute temperature. The viscosity ratio is therefore equal to the temperature ratio T_j/T_0 to a power and for convenience the curves are identified by the temperature ratio T_j/T_0 in figure 10. When the values of φ_3 shown in figure 9 and the same exponents for the remaining parameters are used, the same final correlation curve shown in figure 10 is obtained for the other two jet temperatures.

2221

Correlation of Penetration Coefficient $X_2/\sqrt{C}D_j$

The penetration coefficient $X_2/\sqrt{C}D_j$ was correlated with the parameters by means of the previously described method. The final correlation parameter

$$\frac{\varphi_4 \, (\rho_j/\rho_0)^d \, (V_j/V_0)^e}{(s/\sqrt{C}D_j)^f}$$

was obtained as a result of this correlation. The exponent d of the density ratio was found to be a function of the mixing distance to diameter ratio for constant values of width coefficient as shown in figure 11. The velocity-ratio exponent e varied only as a function of the width coefficient as shown in figure 12. The exponent f of the ratio of the mixing distance to effective diameter and the term φ_4 shown in figures 13 and 14, respectively, are functions of the width coefficient for constant values of the temperature ratio.

The correlation curve of penetration coefficient as a function of the final parameter is shown in figure 15. Much of the scatter in figure 16 results from the difficulty in determining X_2 from the temperature profiles, particularly for the small-diameter jets at the middle and rearmost rake positions. In most instances, the actual values of X_2 are so small (1 in.) that small difference in reading the

temperature and fairing the profiles resulted in errors as high as 20 percent in X_2. Several sets of data were taken under the same conditions to determine the reproducibility of the data. Although the profiles were similar, particularly in the upper region (M_U and X_1), the values of X_2 varied about 10 percent because of the instability of the jet in the lower region. Although these errors in X_2 are large percentagewise, the actual error in the over-all profile should not preclude its practical usefulness.

2221

Correlation of Slope Coefficients

In previous discussion of the profile characteristics, it was noted that the upper and lower slopes of the profiles were independent of jet-pressure ratio for pressure ratios greater than 1.87. The slopes are therefore independent of density ratio, and its effect need not be considered in the analysis. In addition, because the jets are choked, the jet velocity is constant for a given jet total temperature and, hence, the velocity ratio is constant for a particular tunnel velocity. All the data obtained at one rake station for a single jet diameter, jet total temperature, and free-stream velocity may therefore be represented by a single value. Proceeding with the analysis from this point leads to the final correlation parameter $(V_j/V_0)^{0.65}$ (s/D_j) (w/D_j) for the upper-slope coefficient M_U $(T_j-T_0)/D_j$ as shown in figure 16. The final correlation parameter for lower slope coefficient M_L $(T_j-T_0)/D_j$ was found to be $(s/D_j)^{1.25}$ $(V_j/V_0)^{0.53}$ as shown in figure 17.

Correlation of Maximum Temperature Rise Coefficient

In the previous discussion of profile characteristics, the temperature rise at a given rake station was shown to be nearly independent of jet-pressure ratio for a particular jet diameter, jet temperature, and free-stream velocity. The temperature rise decreases slightly with decreasing pressure ratio (fig. 2(a)). Because the flow coefficient also decreases slightly with decreasing pressure ratio (reference 3), the coefficient $\Delta T_m/C\ (T_j-T_0)$ was investigated and found to be independent of density ratio; it was therefore correlated with the remaining parameters. A further simplification of the analysis resulted when it was found that $\Delta T_m/C\ (T_j-T_0)$ was independent of velocity ratio at a particular rake station and jet temperature. A plot of $\Delta T_m/C\ (T_j-T_0)$ was therefore made as a function of the mixing distance to diameter

ratio s/D_j and an independent curve was obtained for each jet diameter. Further analysis of these data showed that if the coefficient $\Delta T_m/C\ (T_j-T_0)$ was multiplied by the width coefficient (w/D_j), a single curve was obtained for all jet temperatures as shown in figure 18. The maximum temperature-rise coefficient $\Delta T_m w/\left[CD_j\ (T_j-T_0)\right]$ is therefore a function only of the mixing distance to diameter ratio.

2221

Comparison of Calculated and Experimental Profiles

The correlation of the penetrations, slopes, and maximum temperature rise with the flow and geometric parameters presented in the foregoing discussion provides a means for obtaining an approximation of the temperature profile.

A number of profiles were calculated, based on the experimental conditions, and compared with the actual profiles. Some typical results are shown in figure 19. A study of these figures shows that the penetration X_1, the upper slope M_U, and the temperature rise ΔT_m are in satisfactory agreement with the experimental profile. The penetration X_2 and the lower slope M_L show lesser agreement because, as previously mentioned, good reproducibility of these data is difficult to obtain. In general, however, the approximate solution is in good agreement with the experimental data and provides a reasonably simple method for obtaining the temperature profile.

Although the results presented in this report are for pressure ratios greater than the choking value of 1.87, the investigation included data at pressure ratios below 1.87. These data are not shown in the curves because of the method of correlation used. An analysis of the limited data obtained at the lower pressure ratios has shown that by using the method presented herein, reasonably good agreement was obtained between the calculated and experimental profiles for a range of jet-pressure ratios from 1.2 to 1.87. A typical example is shown in figure 20.

Boundary-layer removal was employed throughout the investigation; therefore the effect of boundary-layer thickness on the temperature profile was not determined. For most practical applications, however, it is probable that the effect of boundary-layer thickness on the temperature profile is quite small and need not be considered.

EXTRAPOLATION OF RESULTS TO WIDER RANGE OF VARIABLES

The usefulness of the correlations previously given is restricted primarily by the range of variables investigated. It may be possible, however, to utilize the results given outside the range of variables investigated and obtain reasonably good results.

For most practical applications, the greatest restriction of the method results from the limited range of width coefficients investigated. It should be obvious that the effect of width coefficient on the correlation parameters should decrease with increasing values of width coefficient and finally become negligible for a jet expanding unrestricted.

For example, with a free jet the important dimension would be the width of the jet boundary rather than the width of a duct. If the width of the jet boundary at the point of interest can be determined, it should be possible to use a width coefficient based on the jet width to determine the temperature profile.

Although no data are available on the spreading characteristics of jets directed perpendicularly to an air stream, there are some data in the literature on the spreading characteristics of jets directed parallel to an air stream. Because a jet directed perpendicularly is turned very rapidly by the air stream, the expansion of a perpendicularly directed jet probably closely approximates that of a jet directed parallel to an air stream. If this assumption is made, the spreading characteristics of a jet directed perpendicularly to an air stream can be calculated by the method of reference 4. The results of reference 4 were based on the turbulent mixing of an incompressible fluid.

The width of the jet boundary, as determined in reference 4, is the momentum width rather than the thermal width. The thermal width, however, can be simply obtained from turbulent-mass and heat-exchange considerations, wherein the ratio of thermal width to momentum width has been found to equal $\sqrt{2}$ (reference 5). The thermal expansion of a free jet, calculated on this basis, is shown in figure 21 where the jet width coefficient w/D_j is shown as a function of mixing distance to diameter ratio s/D_j for several velocity ratios.

Before calculating the various parameters necessary for obtaining the temperature profile, it is advisable to first determine the jet width coefficient at the point in question. If, for the problem being considered, the jet width coefficient as determined from figure 21 is greater than the duct width coefficient, the duct width coefficient is the important parameter. If the jet width coefficient is less than the duct width coefficient, the jet is relatively unrestricted and the jet width coefficient becomes the important parameter and should be used in the calculations.

CONCLUDING REMARKS

A method that provides a reasonably simple means of obtaining the approximate temperature profile downstream of a heated-air jet directed perpendicularly to an air stream has been presented. The solution is presented in terms of dimensionless parameters of the flow and the geometric conditions.

Lewis Flight Propulsion Laboratory
National Advisory Committee for Aeronautics
Cleveland, Ohio, April 30, 1951

2221

REFERENCES

1. Callaghan, Edmund E., and Ruggeri, Robert S.: Investigation of the Penetration of an Air Jet Directed Perpendicularly to an Air Stream. NACA TN 1615, 1948.

2. Ruggeri, Robert S., Callaghan, Edmund E., and Bowden, Dean T.: Penetration of Air Jets Issuing from Circular, Square, and Elliptical Orifices Directed Perpendicularly to an Air Stream. NACA TN 2019, 1950.

3. Callaghan, Edmund E., and Bowden, Dean T.: Investigation of Flow Coefficient of Circular, Square, and Elliptical Orifices at High Pressure Ratios. NACA TN 1947, 1949.

4. Squire, H. B., and Trouncer, J.: Round Jets in a General Stream. Rep. Aero. 1904, British R.A.E., Jan. 1944.

5. Szablewski, W.: The Diffusion of a Hot Air Jet in Air in Motion. NACA TM 1288, 1950.

1777

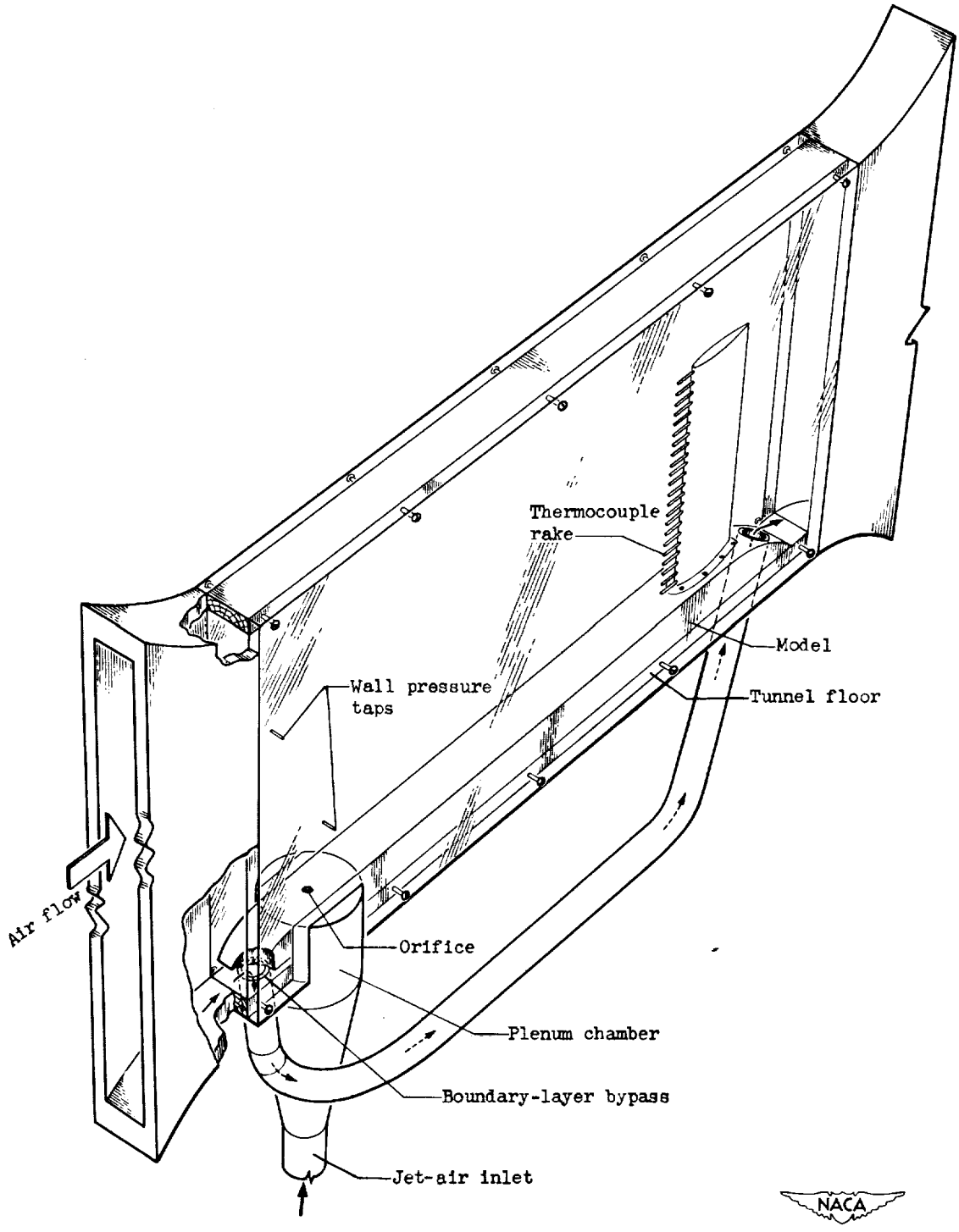

Figure 1. - Arrangement of orifice in plane parallel to air stream.

RT/T-554

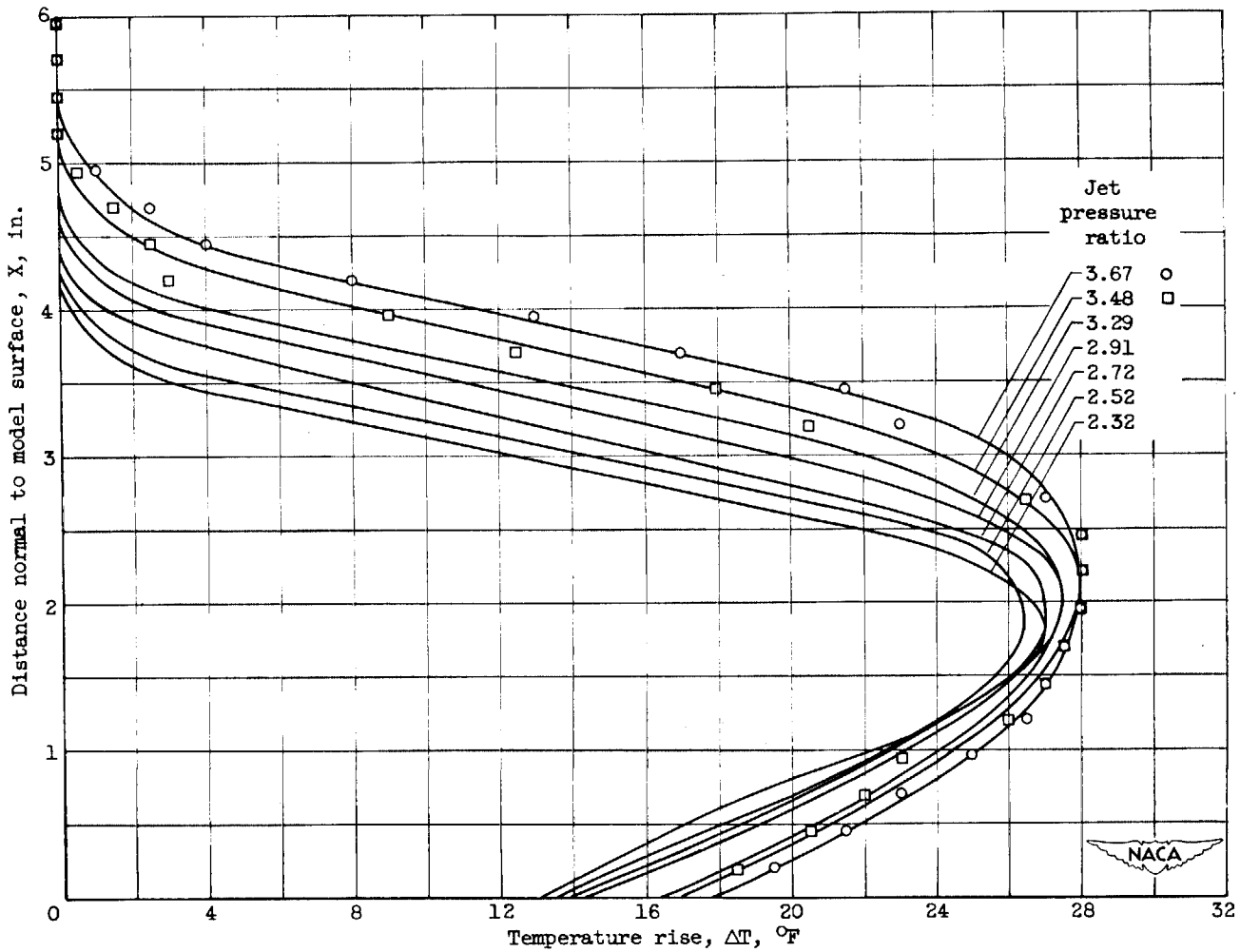

(a) Typical profiles obtained at 11.81-inch rake station for various jet pressure ratios. Orifice diameter, 0.385 inch; jet total temperature, 860° R; free-stream velocity, 390 feet per second; free-stream total temperature, 519° R; free-stream static pressure, 25.80 inches of mercury.

Figure 2. - Typical temperature profiles and generalization of profiles.

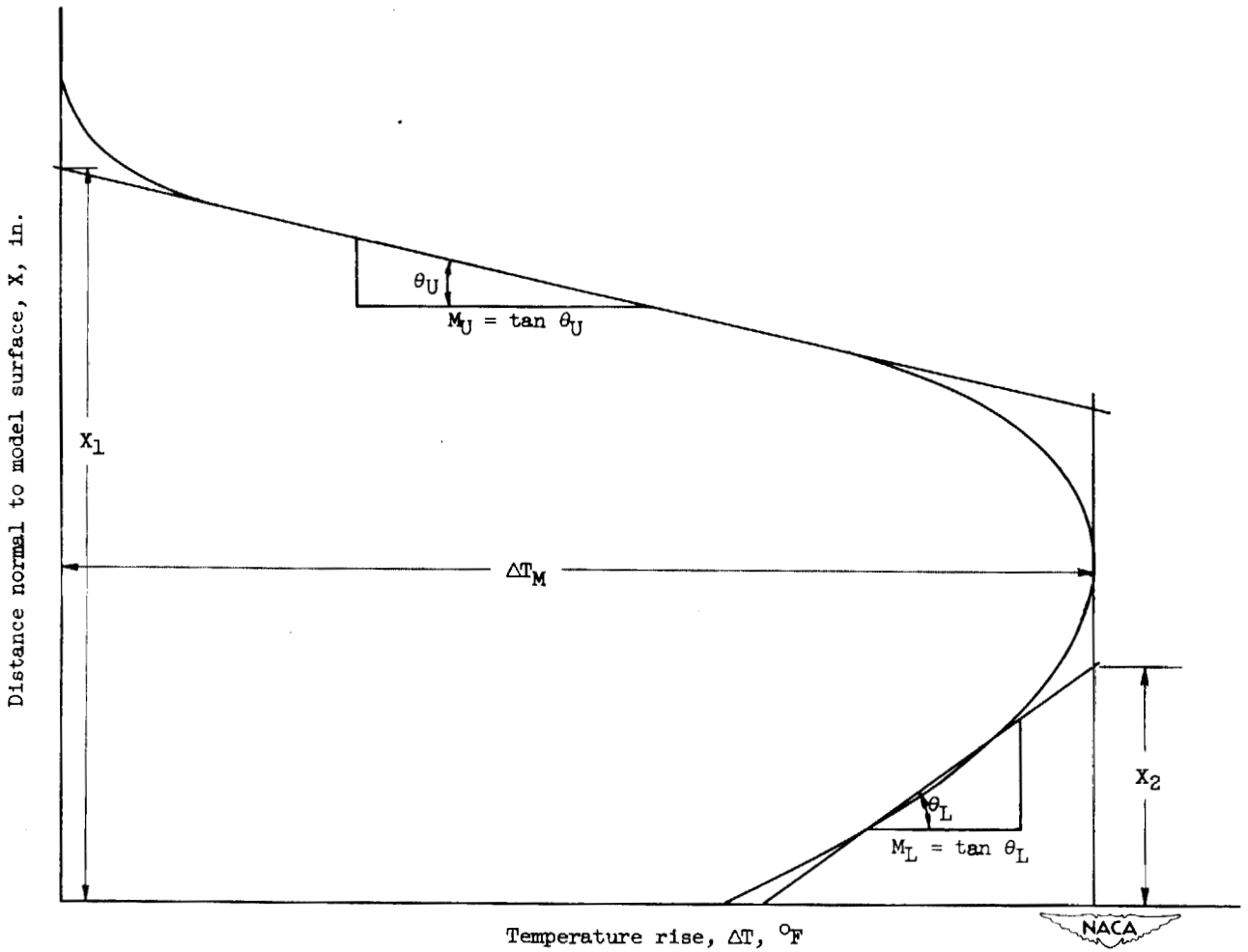

(b) Generalization of profiles showing penetrations X_1 and X_2, slopes M_U and M_L, and maximum temperature rise ΔT_m.

Figure 2. - Concluded. Typical temperature profiles and generalization of profiles.

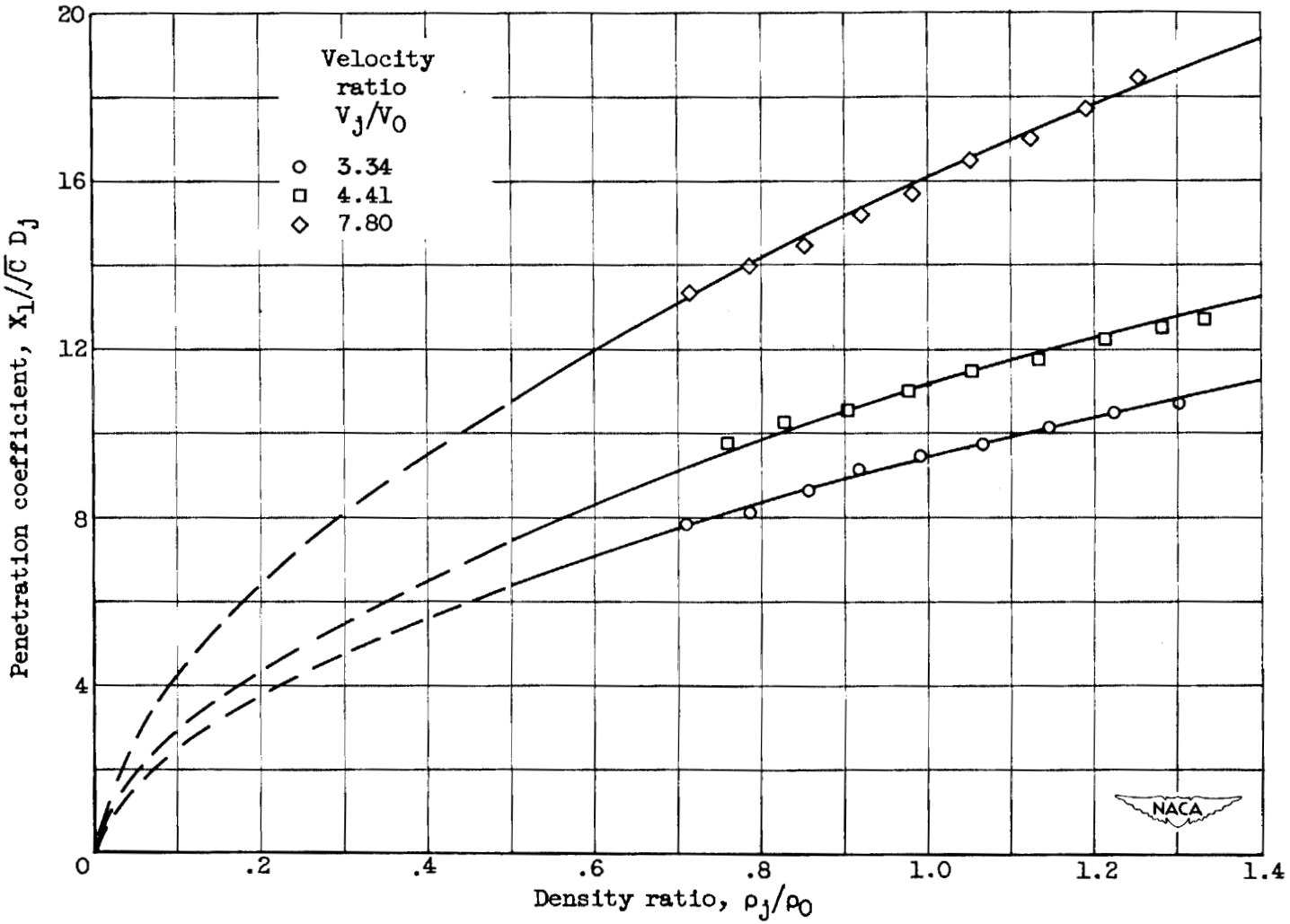

Figure 3. - Variation of penetration coefficient $X_1/\sqrt{C}\ D_j$ with density ratio for several velocity ratios. Orifice diameter, 0.385 inch; jet total temperature, 860° R; rake station, 4.81 inches.

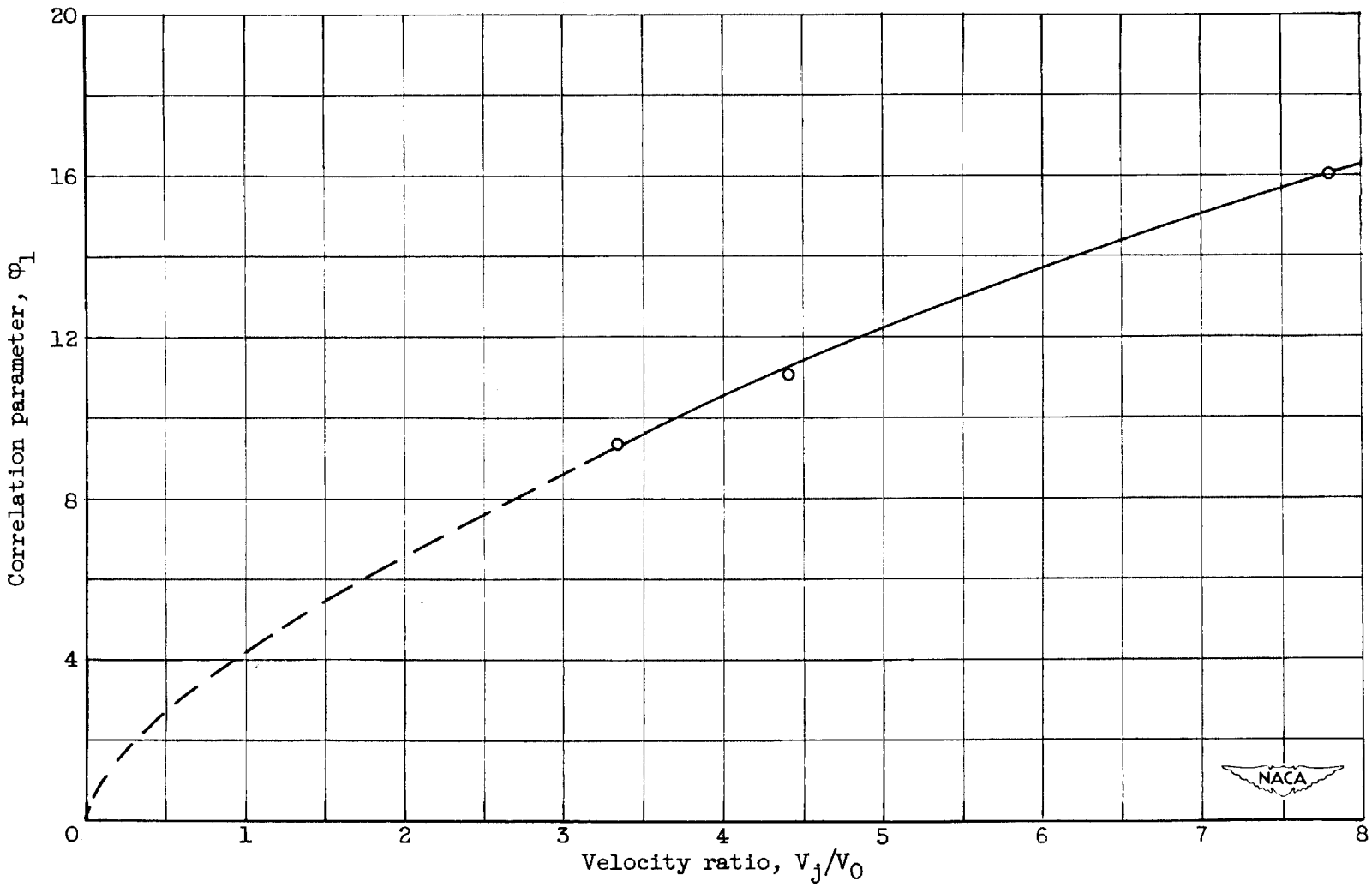

Figure 4. - Variation of correlation parameter φ_1 with velocity ratio. Orifice diameter, 0.385 inch; jet total temperature, 860° R; rake station, 4.81 inch.

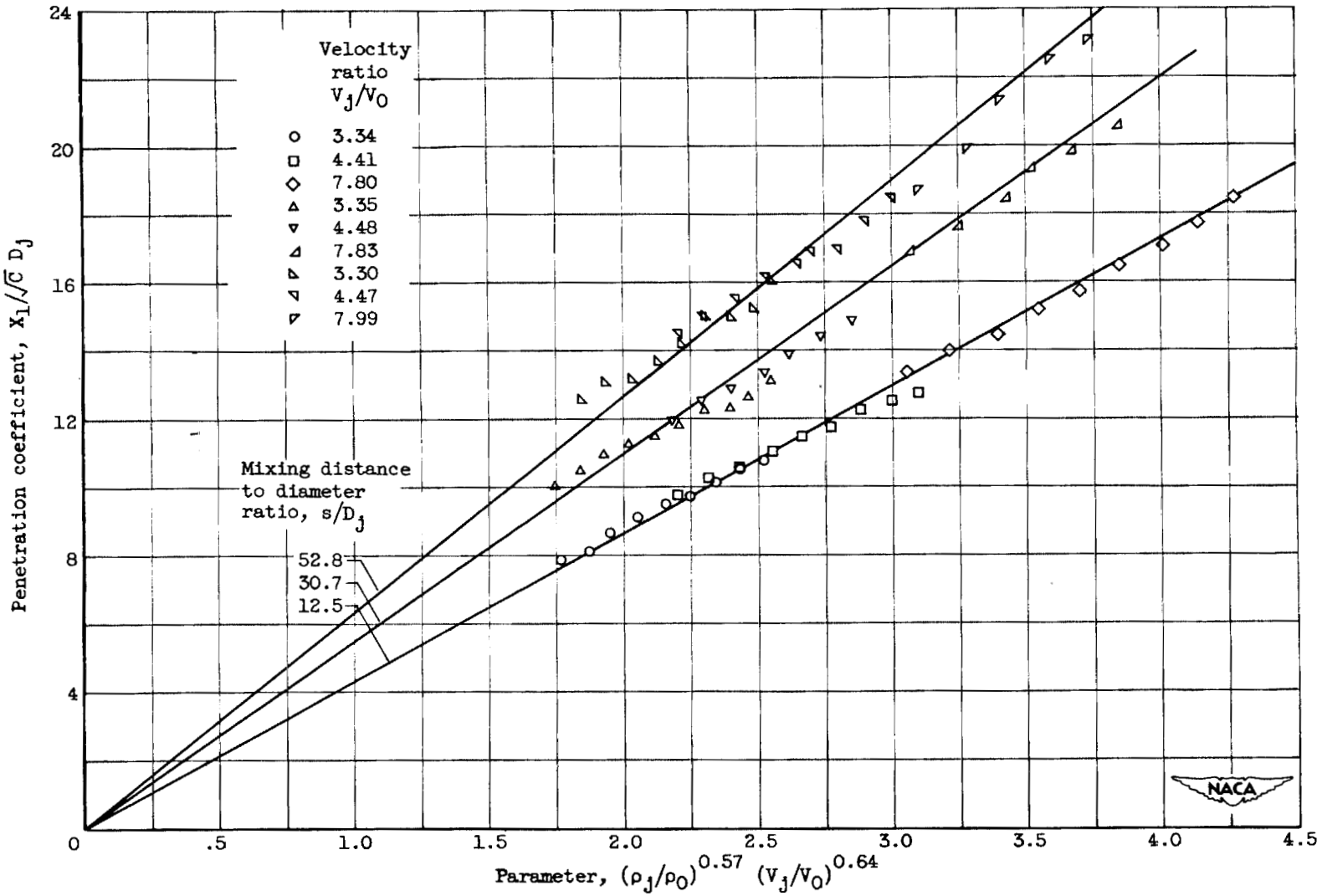

Figure 5. - Variation of penetration coefficient $X_1/\sqrt{C}\ D_j$ with parameter $(\rho_j/\rho_0)^{0.57}\ (V_j/V_0)^{0.64}$ for three mixing distance to diameter ratios. Orifice diameter, 0.385 inch; jet total temperature, 860° R.

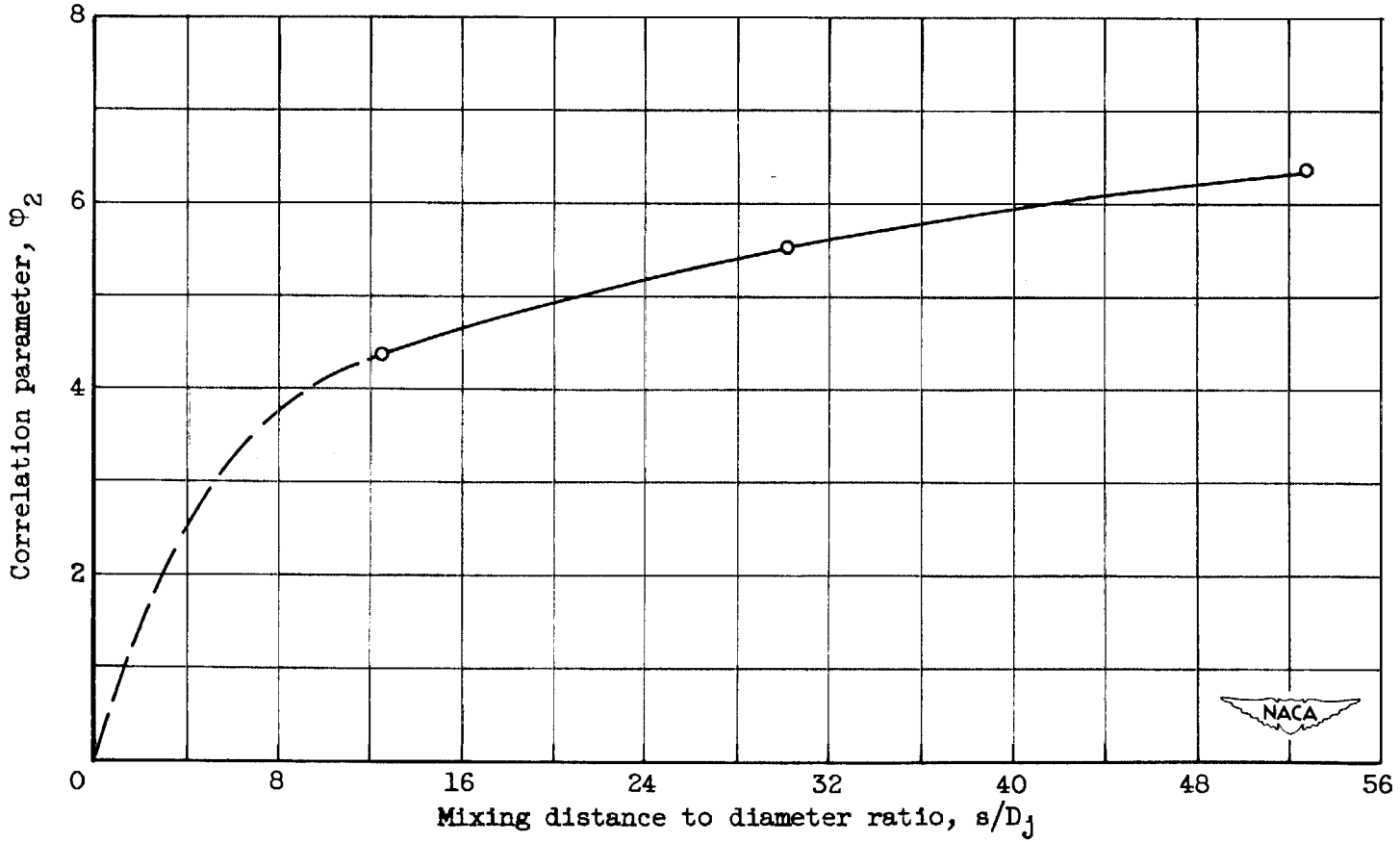

Figure 6. - Variation of correlation parameter φ_2 with mixing distance to diameter ratio. Orifice diameter, 0.385 inch; jet total temperature, 860° R.

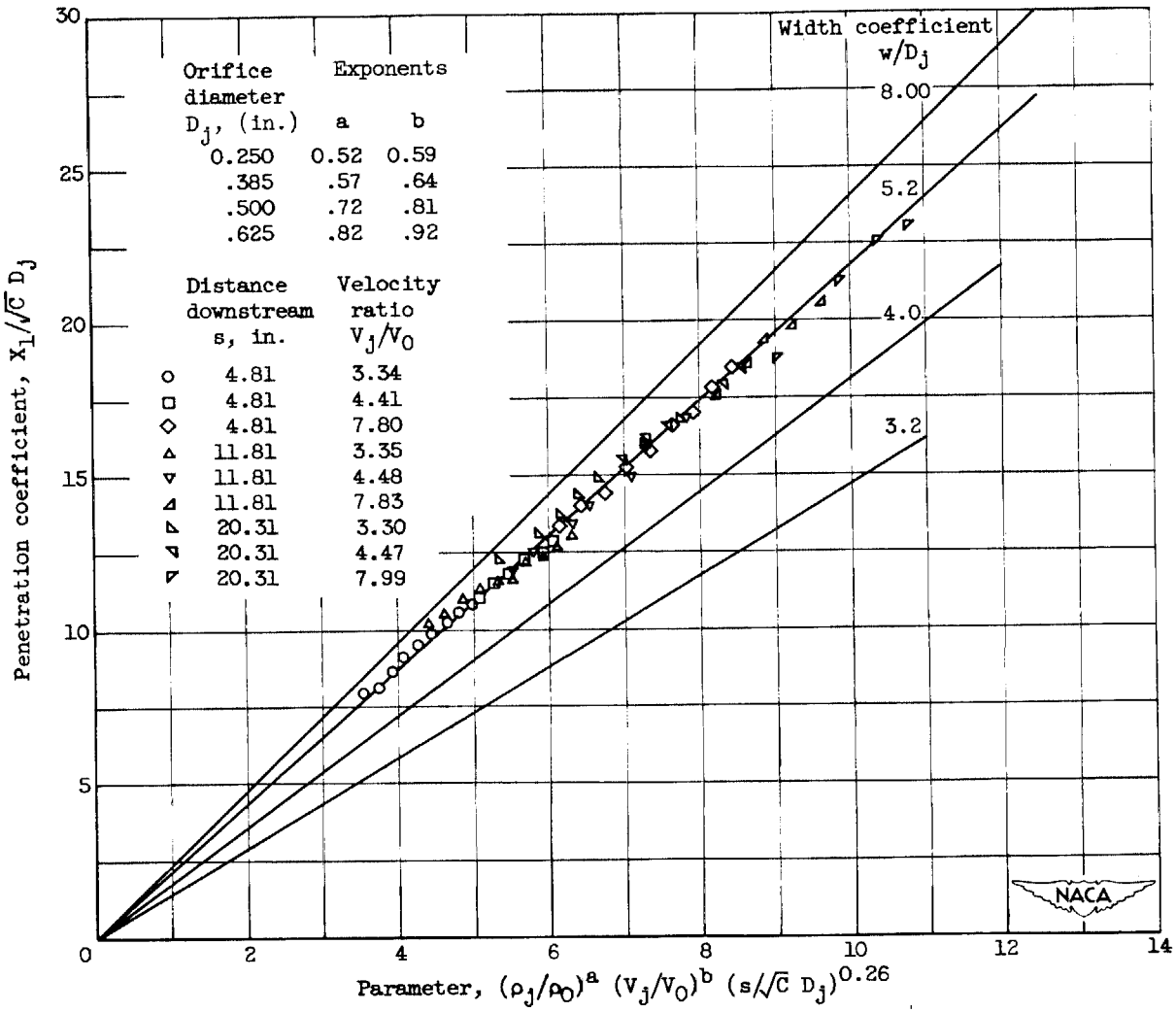

Figure 7. - Variation of penetration coefficient $X_1/\sqrt{C}\ D_j$ with parameter $(\rho_j/\rho_0)^a\ (V_j/V_0)^b\ (s/\sqrt{C}\ D_j)^{0.26}$ for four orifice diameters. Jet total temperature, 860° R.

1777

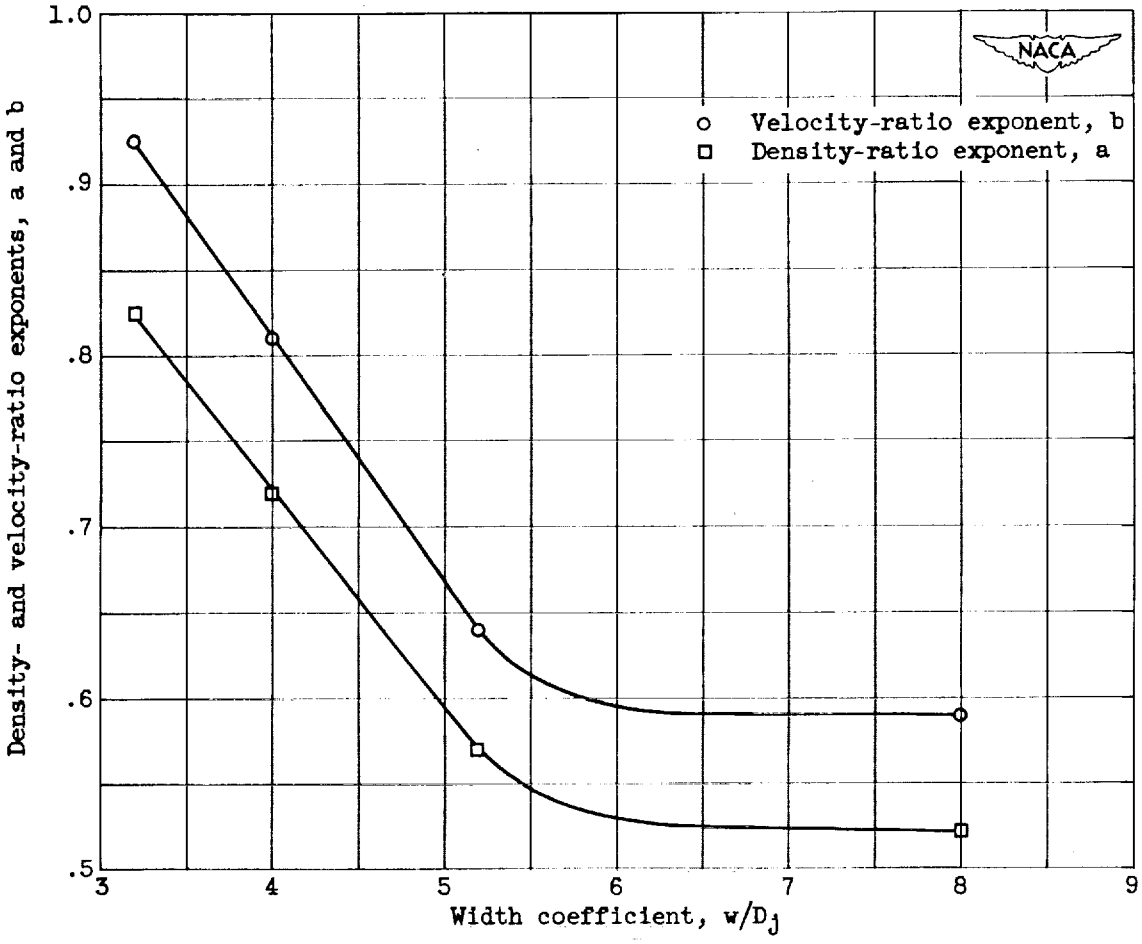

Figure 8. - Variation of density- and velocity-ratio exponents a and b with width coefficient.

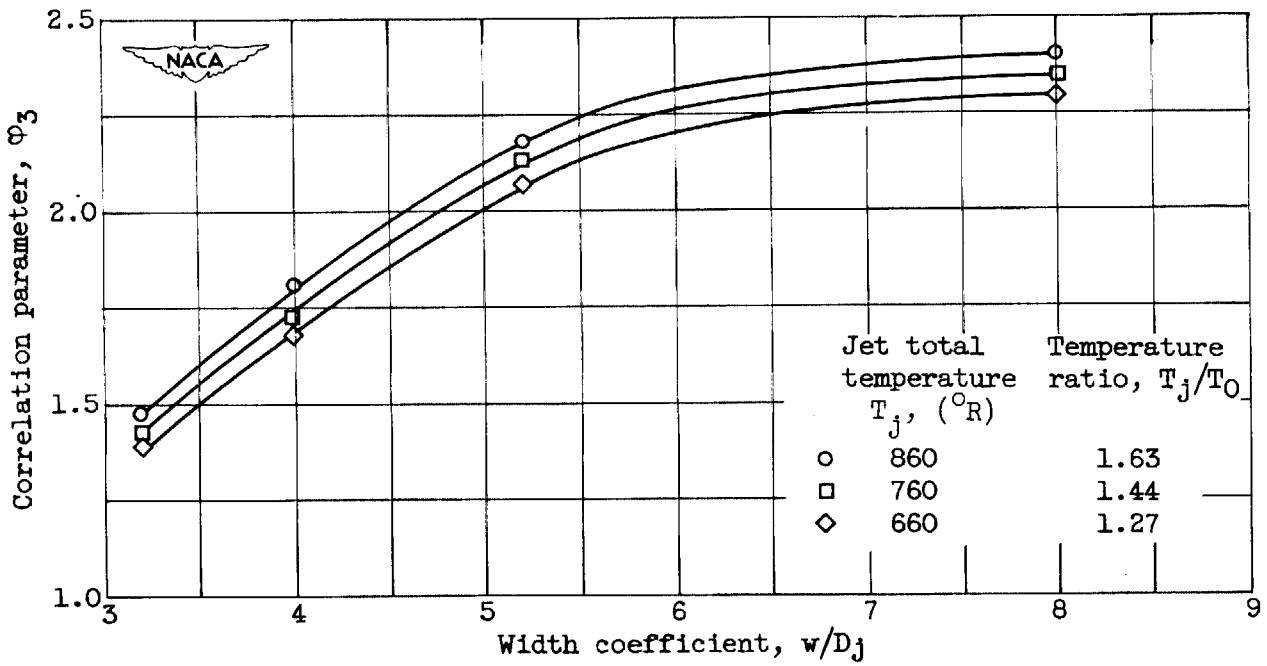

Figure 9. - Variation of correlation parameter φ_3 with width coefficient for various temperature ratios. Jet total temperature, 860° R.

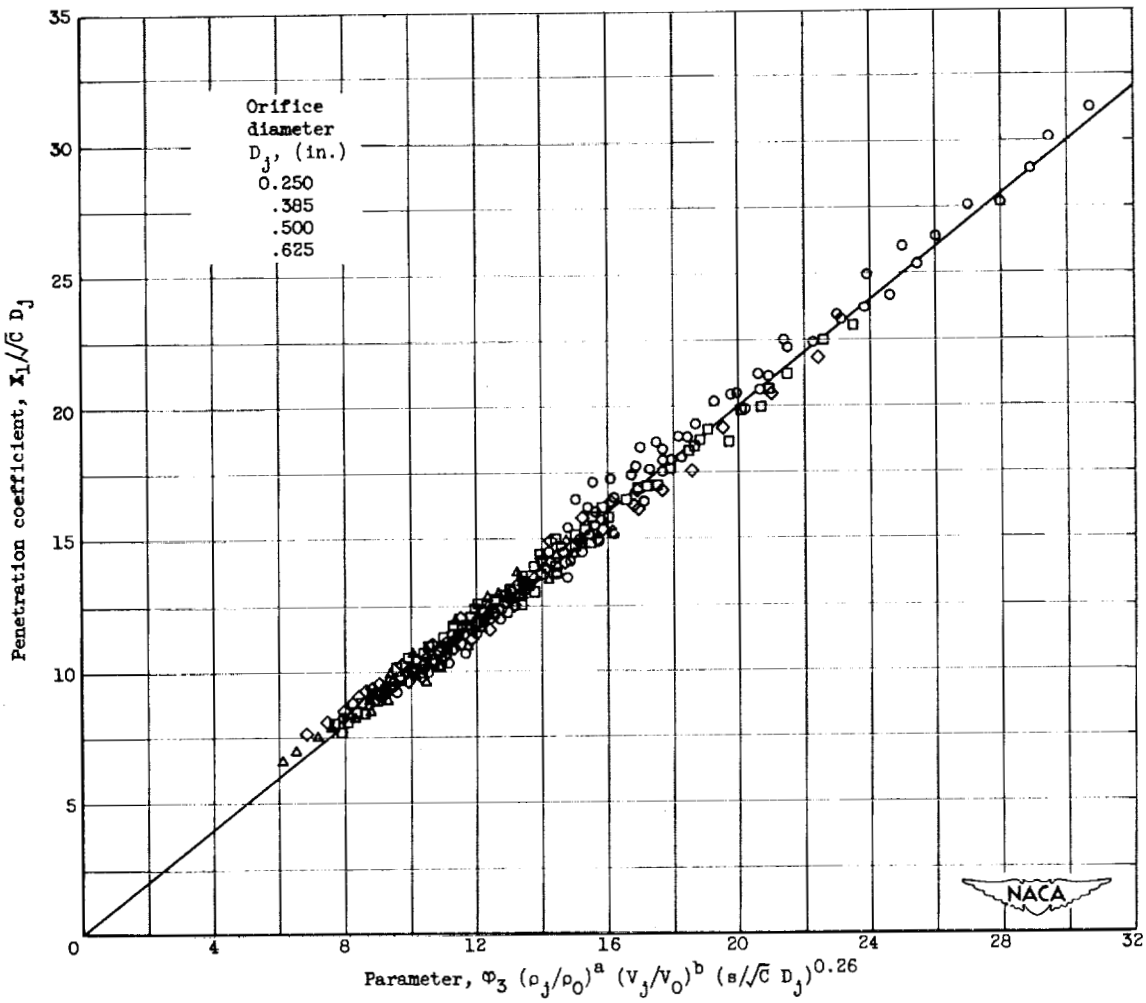

Figure 10. - Variation of penetration coefficient $X_1/\sqrt{C}\ D_j$ with parameter $\varphi_3\ (\rho_j/\rho_0)^a\ (V_j/V_0)^b\ (s/\sqrt{C}\ D_j)^{0.26}$ for various temperature ratios.

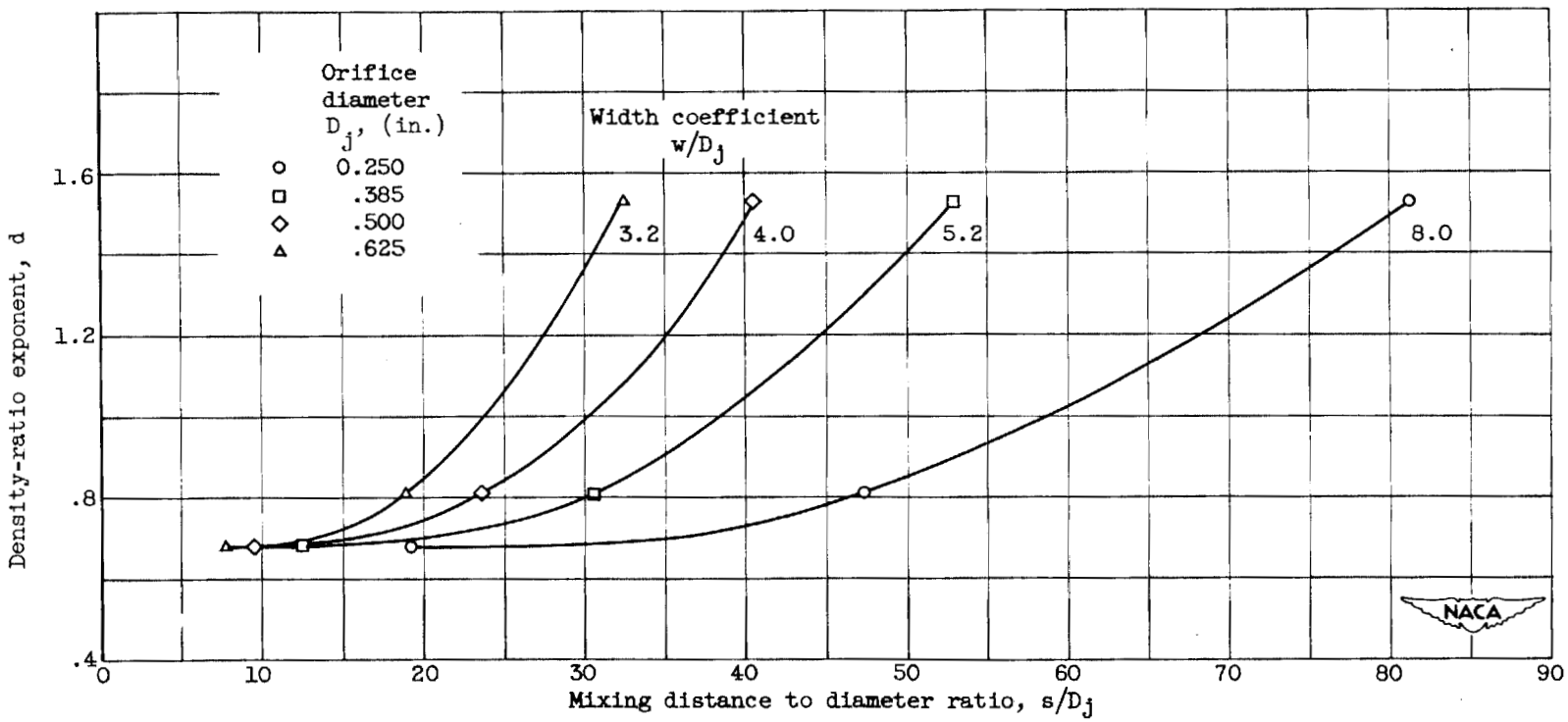

Figure 11. - Variation of density-ratio exponent d with mixing distance to diameter ratio for constant values of width coefficient.

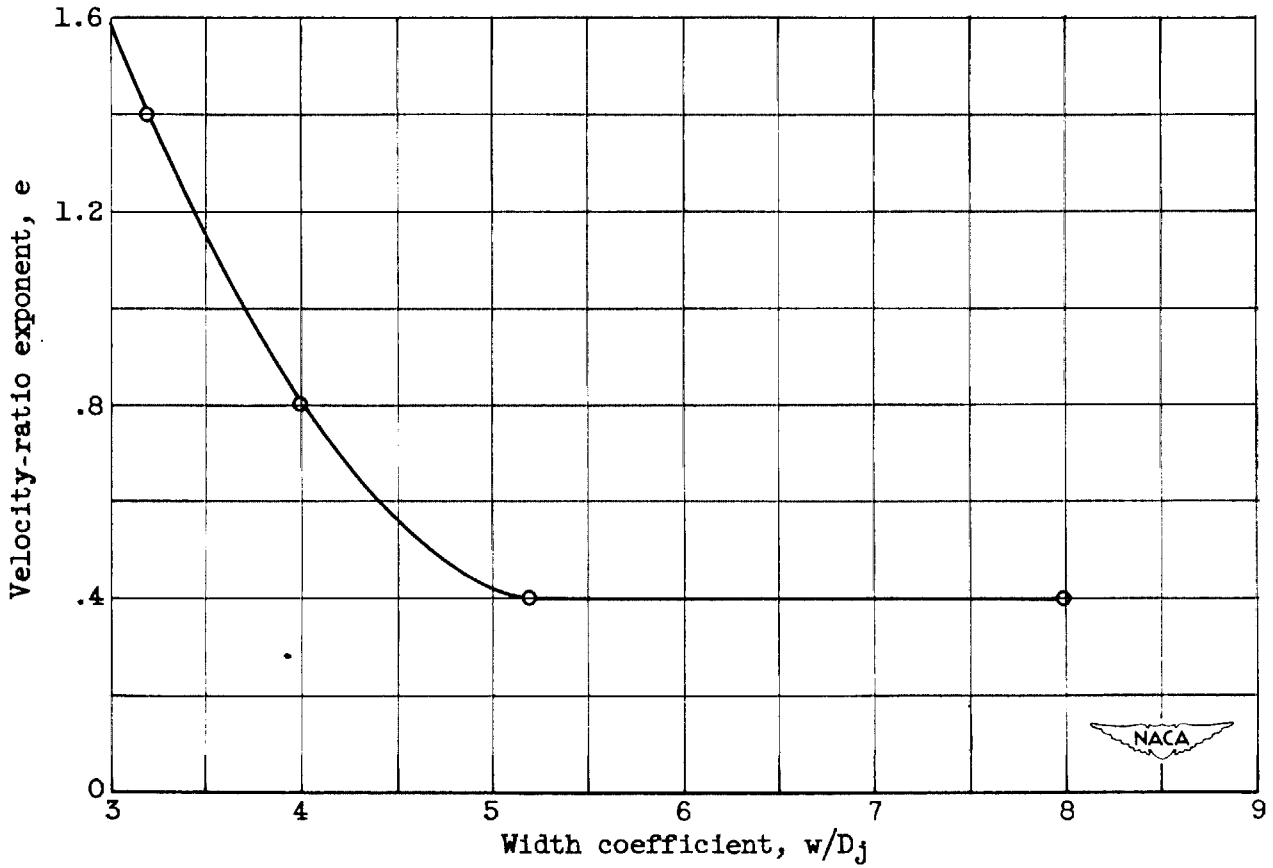

Figure 12. - Variation of the velocity-ratio exponent e with width coefficient.

2221

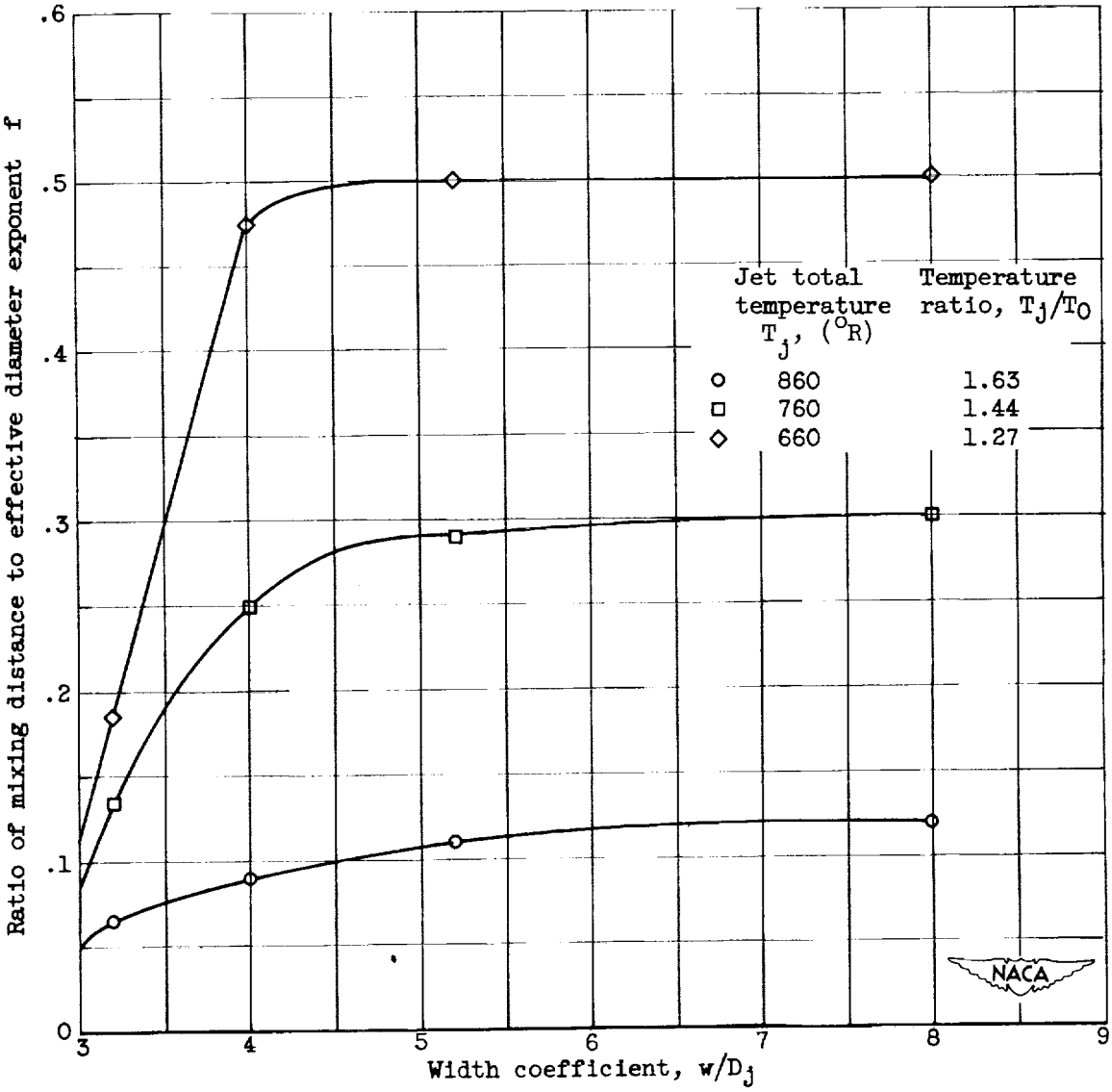

Figure 13. - Variation of ratio of mixing distance to effective diameter exponent f with width coefficient.

2221

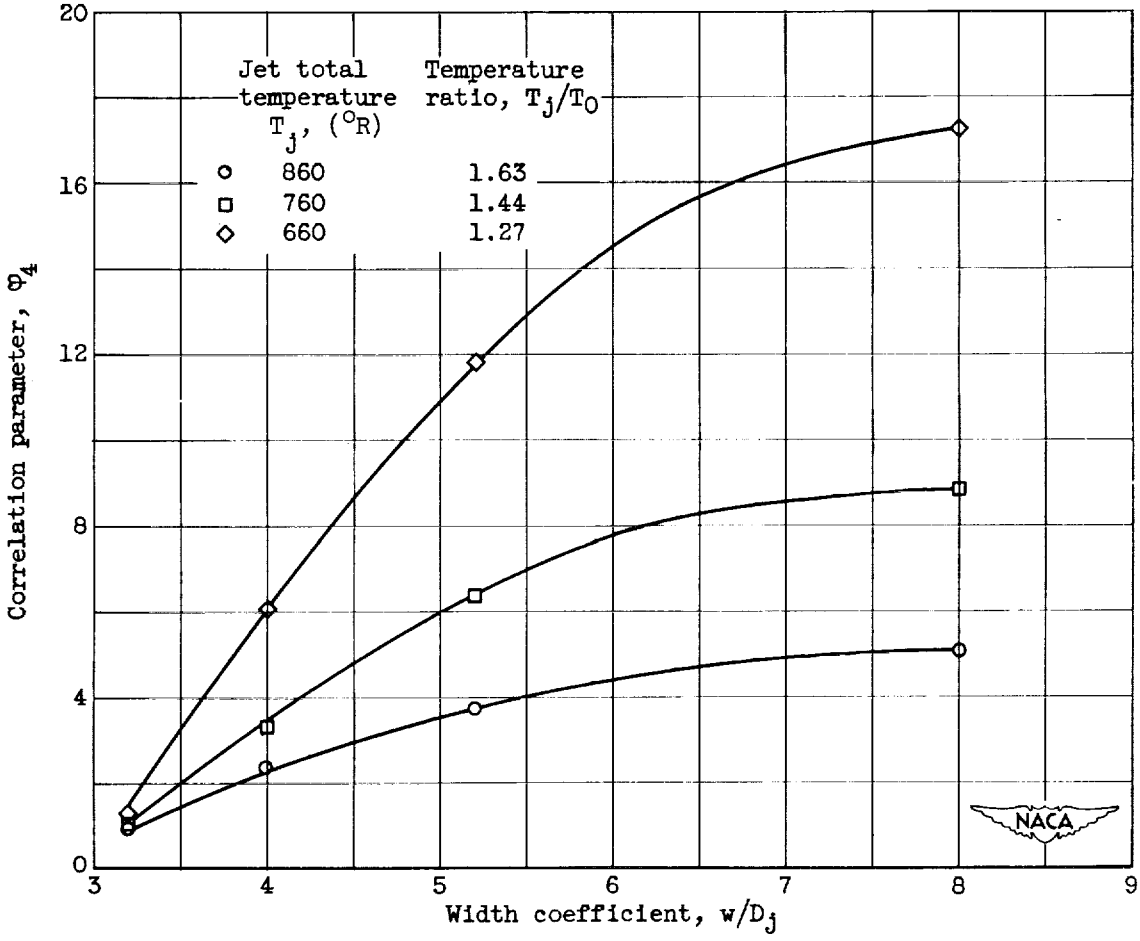

Figure 14. - Variation of correlation parameter Φ_4 with width coefficient for constant values of the temperature ratio.

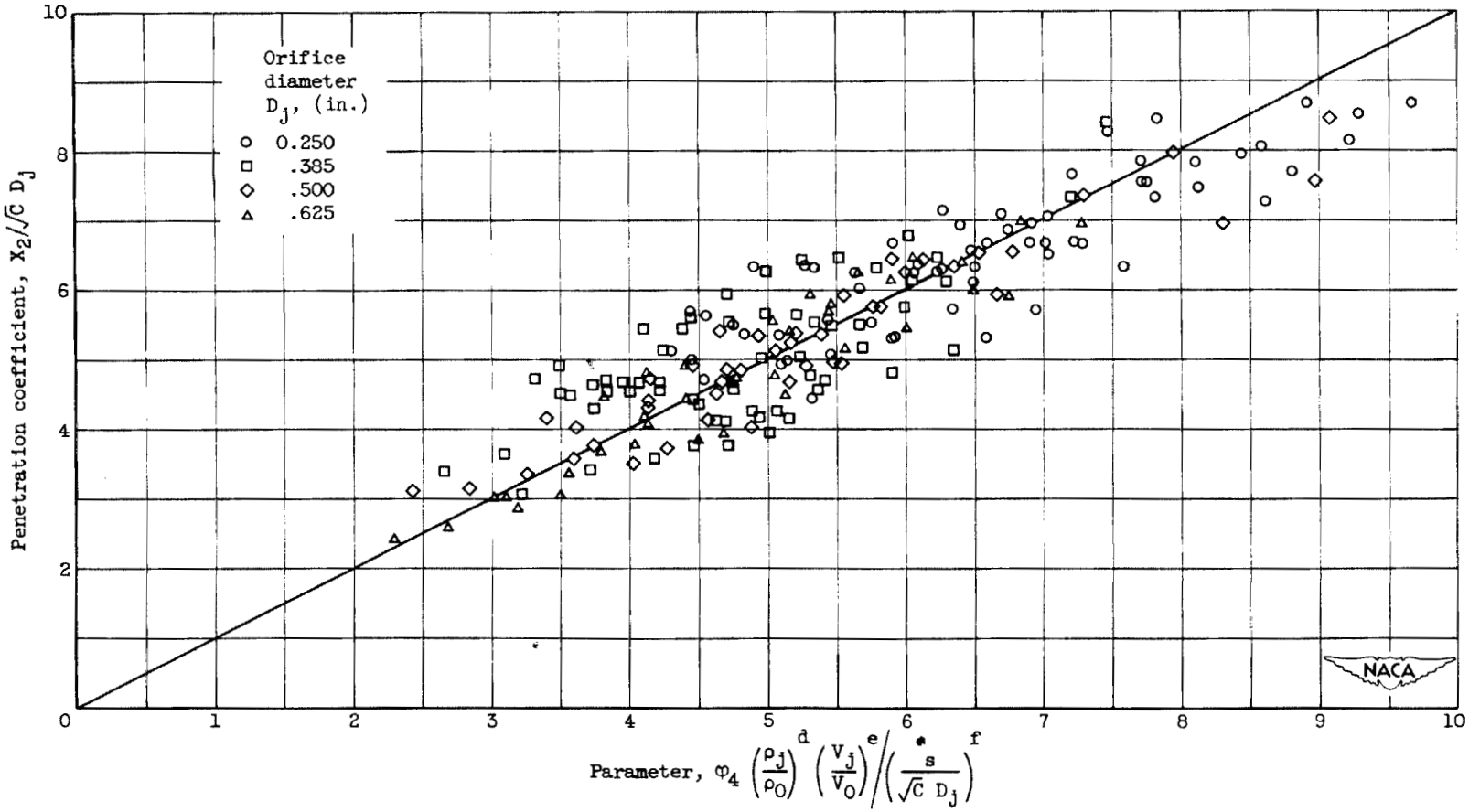

Figure 15. - Variation of penetration coefficient $X_2/\sqrt{C}\ D_j$ with final parameter $\varphi_4 \left(\frac{\rho_j}{\rho_0}\right)^d \left(\frac{V_j}{V_0}\right)^e \Big/ \left(\frac{s}{\sqrt{C}\ D_j}\right)^f$ for various temperature ratios.

2221

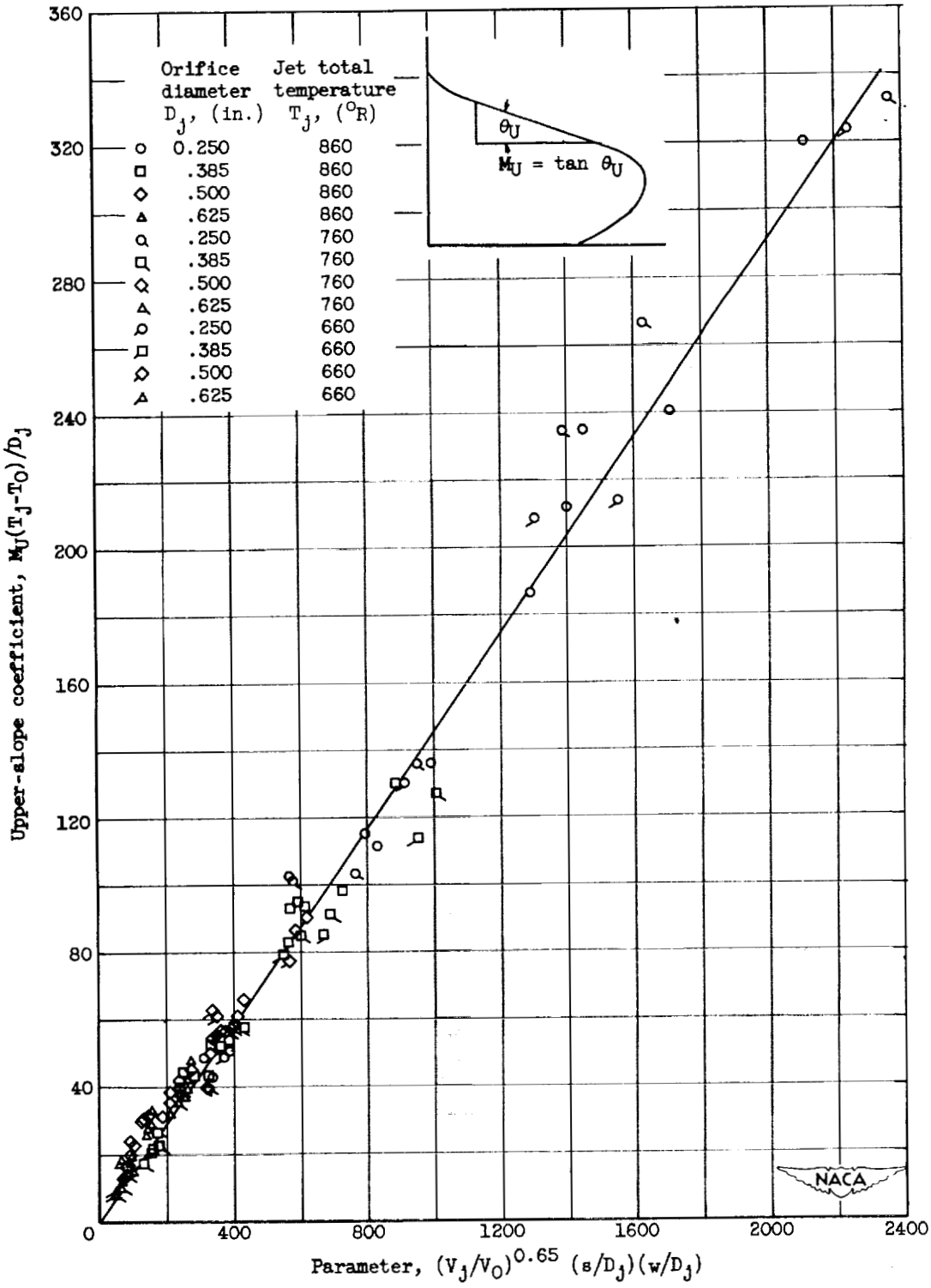

Figure 16. - Variation of upper-slope coefficient $M_U(T_j-T_0)/D_j$ with parameter $(V_j/V_0)^{0.65}(s/D_j)(w/D_j)$.

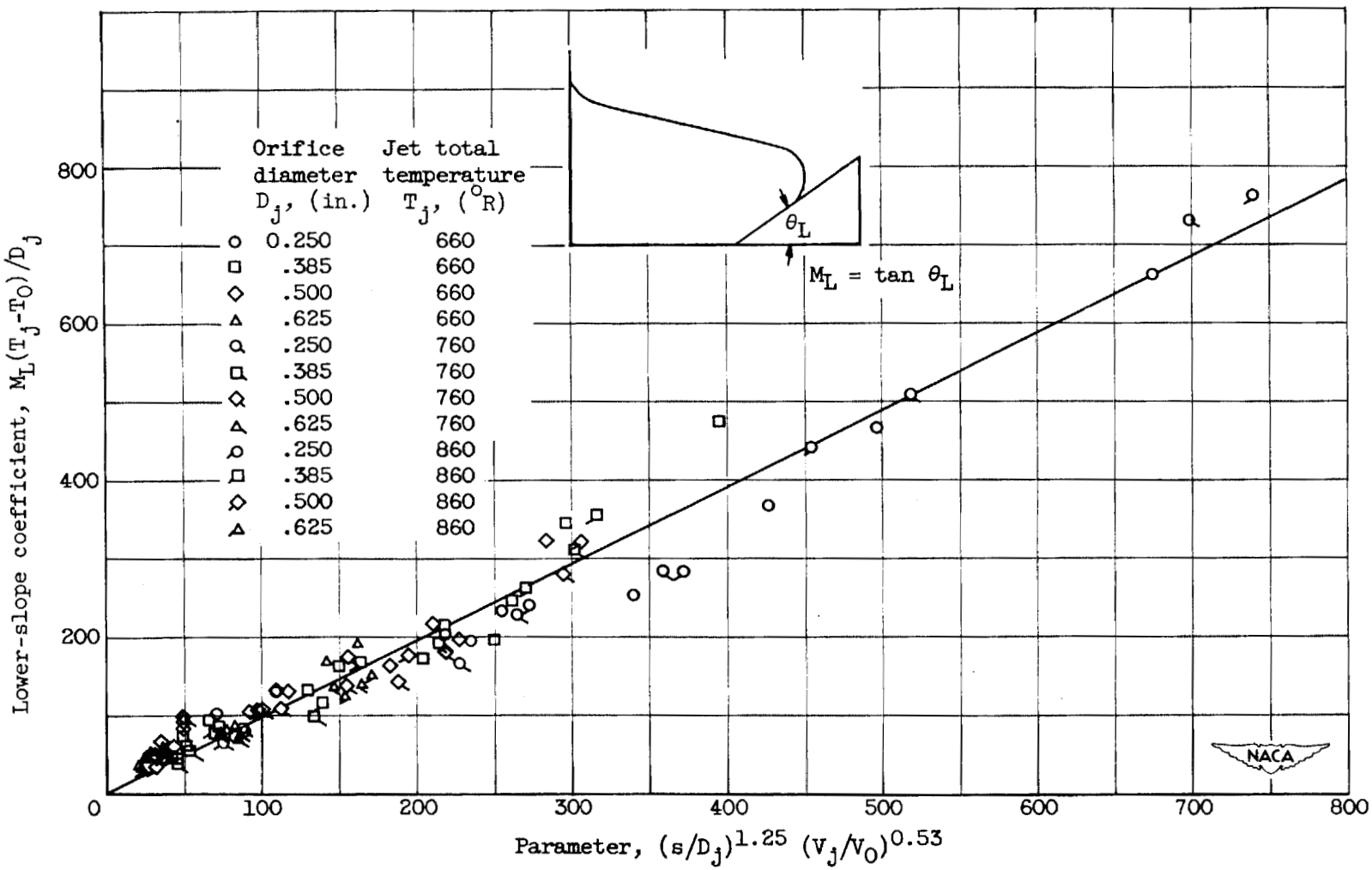

Figure 17. - Variation of lower-slope coefficient $M_L(T_j-T_0)/D_j$ with parameter $(s/D_j)^{1.25} (V_j/V_0)^{0.53}$ for various jet total temperatures.

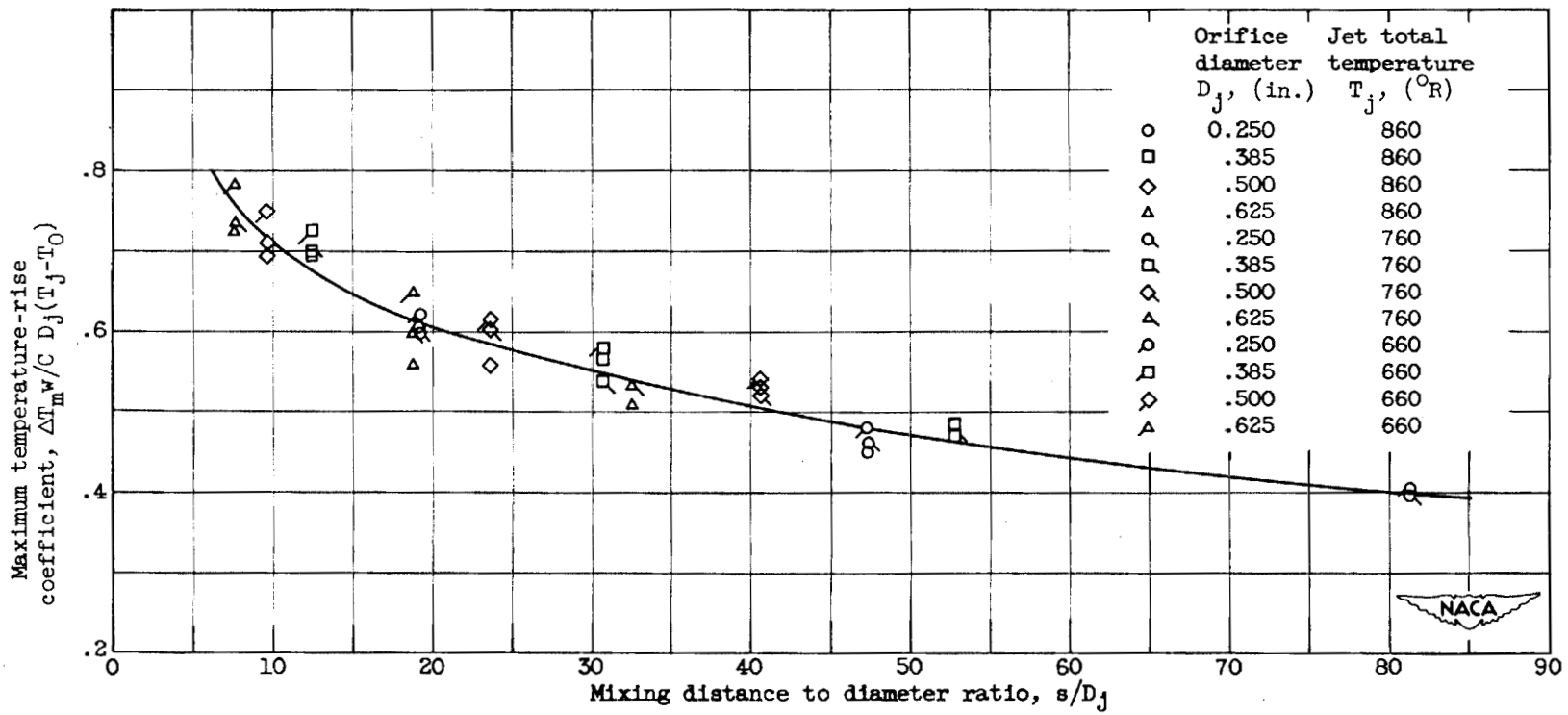

Figure 18. - Variation of maximum temperature-rise coefficient $\Delta T_m w/C\ D_j(T_j-T_o)$ with mixing distance to diameter ratio.

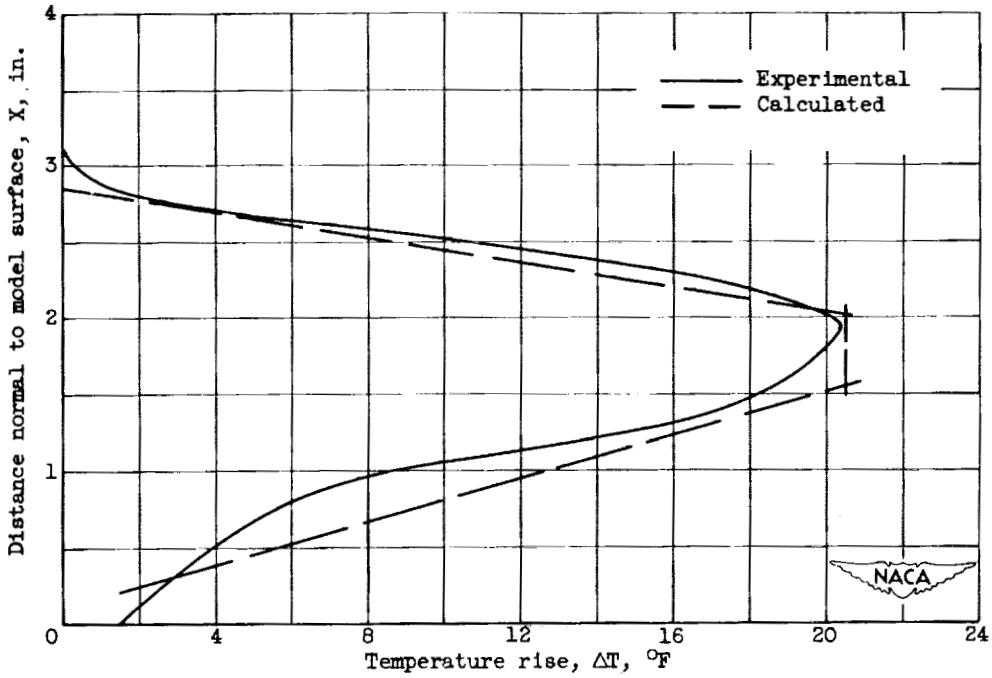

(a) Orifice diameter, 0.250 inch; jet total temperature, 860° R; jet pressure ratio, 3.36; free-stream velocity, 390 feet per second; rake station, 4.81 inches.

Figure 19. - Comparison of calculated and experimental temperature profiles.

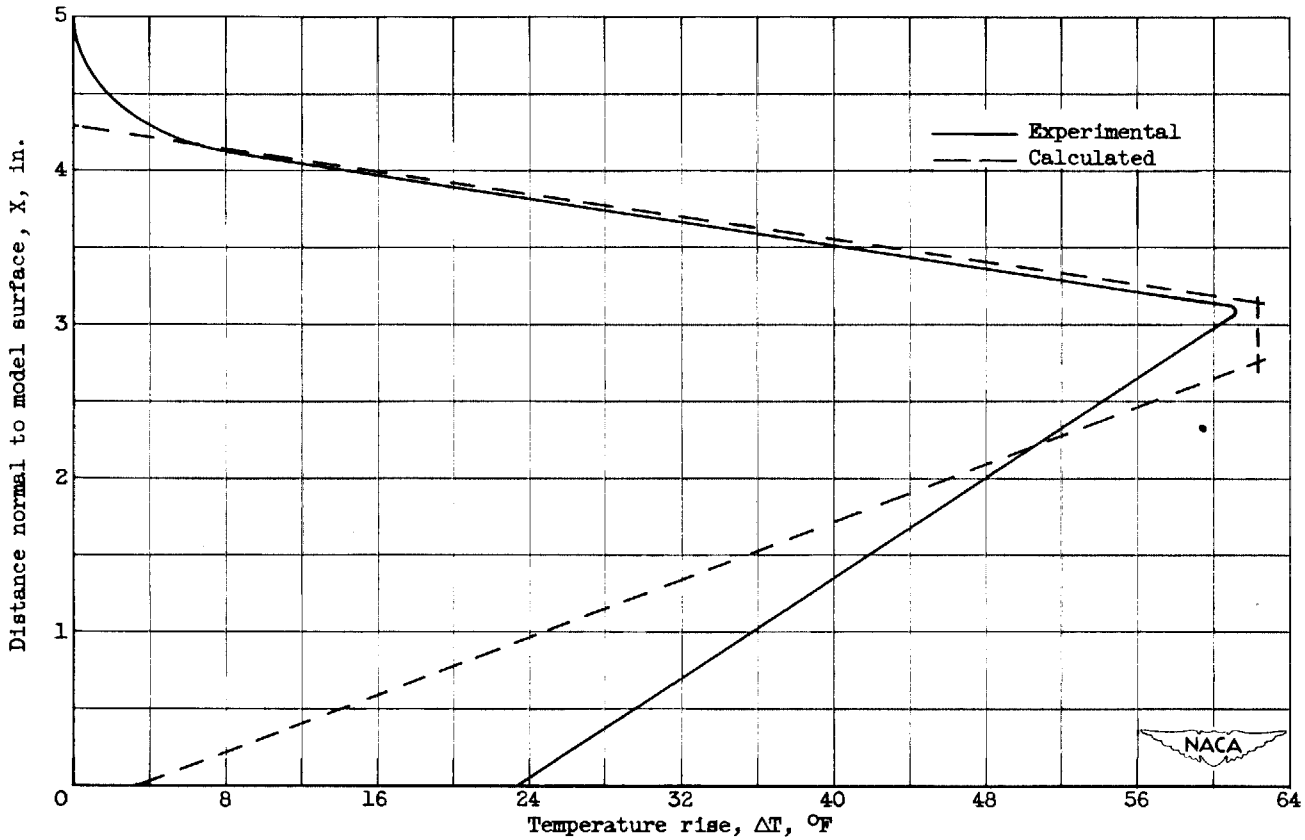

(b) Orifice diameter, 0.625 inch; jet total temperature, 860° R; jet pressure ratio, 2.10; free-stream velocity, 290 feet per second; rake station, 4.81 inches.

Figure 19. - Continued. Comparison of calculated and experimental temperature profiles.

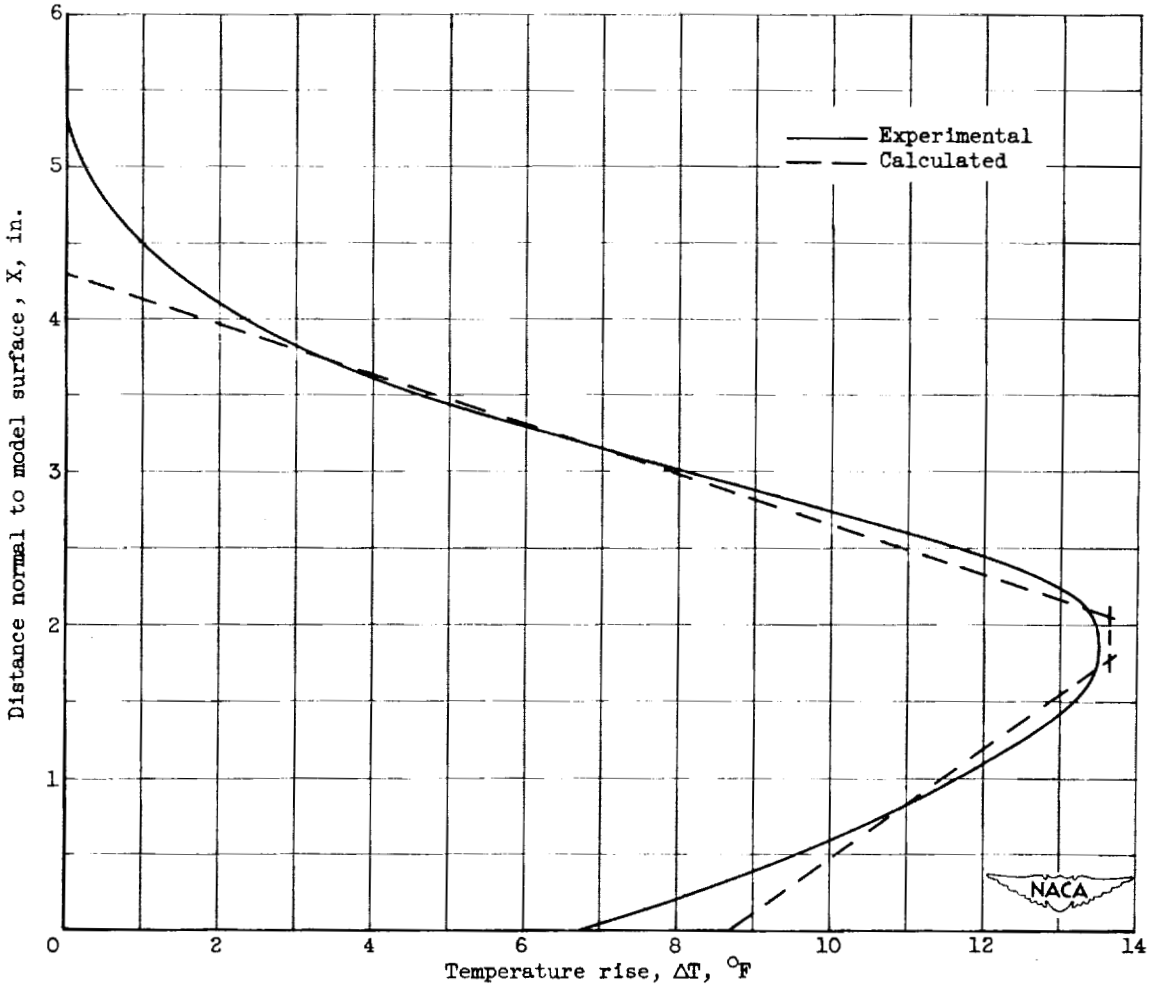

(c) Orifice diameter, 0.250 inch; jet total temperature, 860° R; jet pressure ratio, 3.64; free-stream velocity, 390 feet per second; rake station, 20.31 inches.

Figure 19. - Continued. Comparison of calculated and experimental temperature profiles.

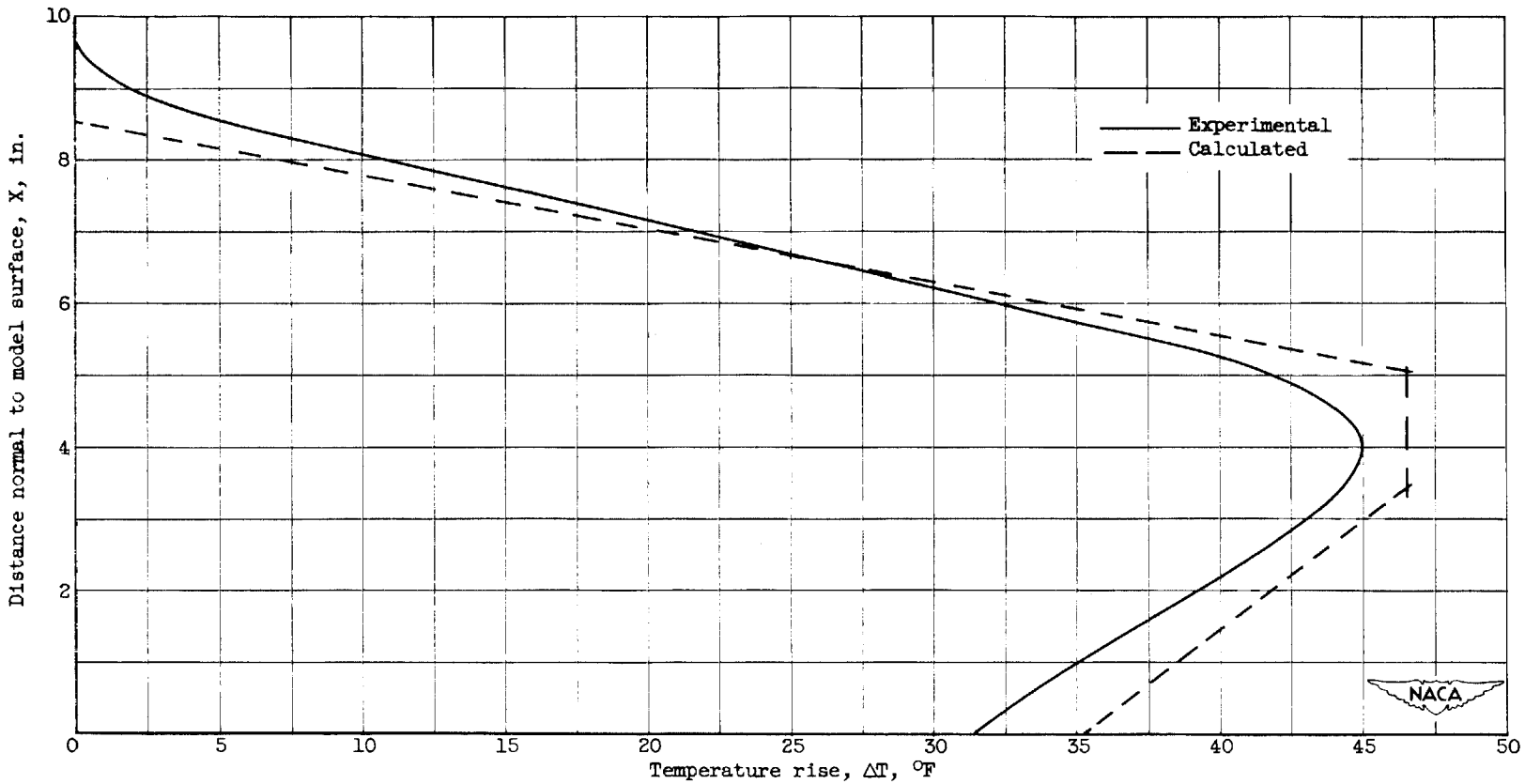

(d) Orifice diameter, 0.625 inch; jet total temperature, 860° R; jet pressure ratio, 2.85; free-stream velocity, 290 feet per second; rake station, 20.31 inches.

Figure 19. - Concluded. Comparison of calculated and experimental temperature profiles.

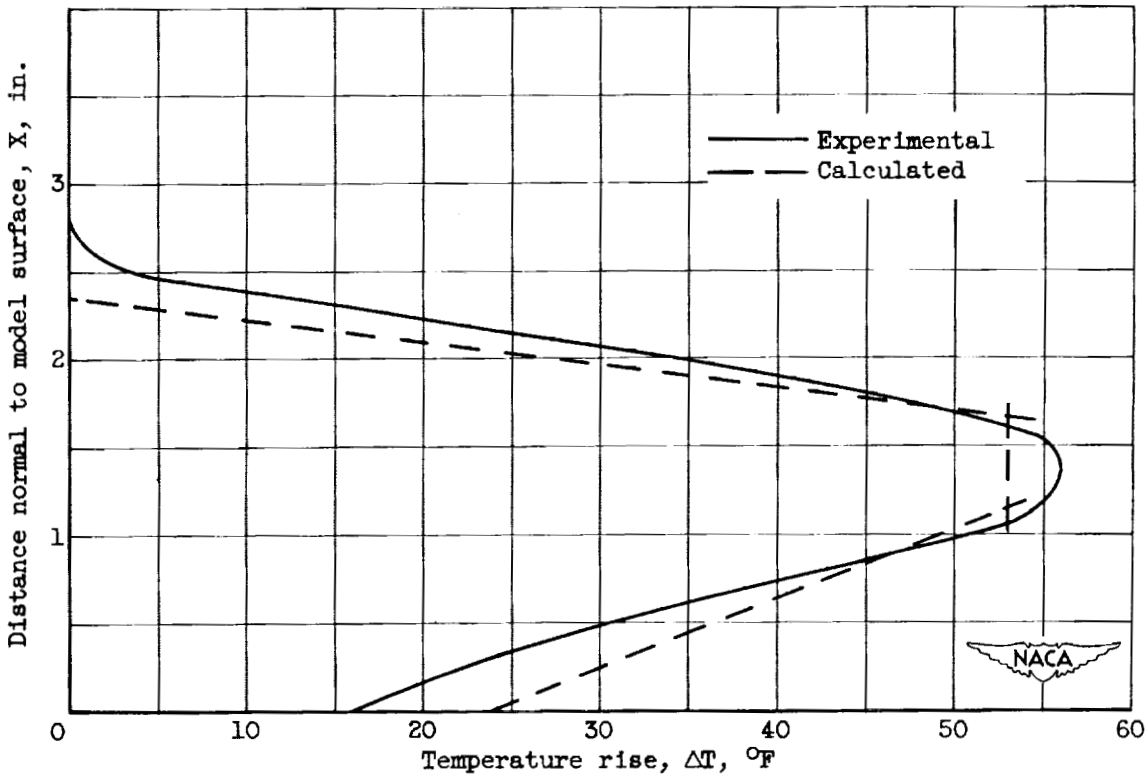

Figure 20. - Comparison of calculated and experimental profile for jet operating at pressure ratio less than choking. Jet pressure ratio, 1.33; orifice diameter, 0.625 inch; jet total temperature, 860° R; tunnel-air velocity, 290 feet per second; rake station, 4.81 inches.

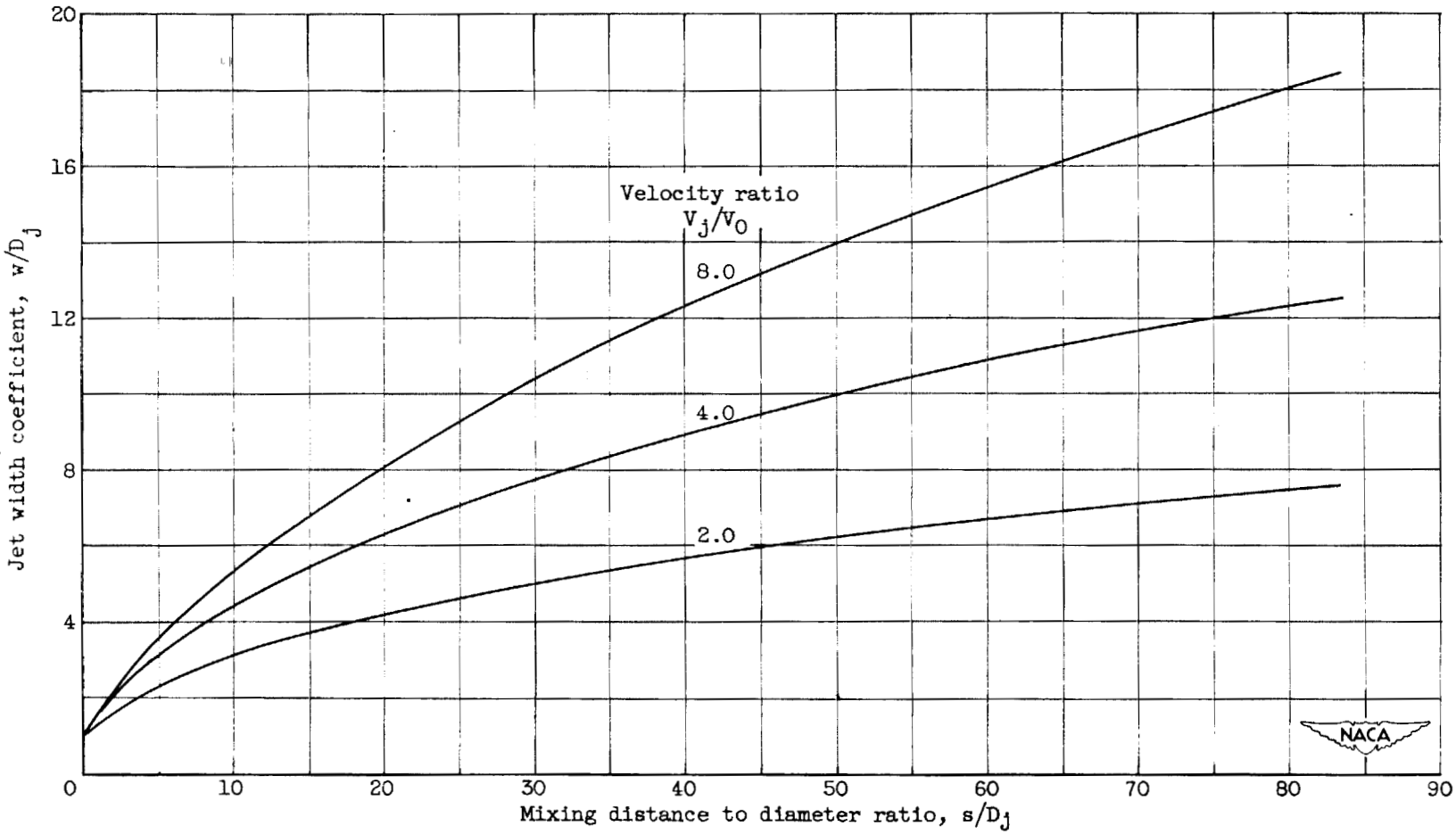

Figure 21. - Variation of jet-width coefficient w/D_j with mixing distance to diameter ratio for three velocity ratios.

NACA-Langley - 9-26-51 - 1000